Uncertainty in visual processes predicts geometrical optical illusions ☆

Cornelia Fermüller [a,*], Henrik Malm [b]

[a] *Department of Computer Science, Computer Vision Laboratory, Center for Automation Research, Institute for Advanced Computer Studies, University of Maryland, College Park, MD 20742-3275, USA*
[b] *Department of Mathematics (LTH), Mathematical Imaging Group (MIG), Lund Institute of Technology/Lund University, P.O. Box 118, S-221 00 Lund, Sweden*

Abstract

It is proposed in this paper that many geometrical optical illusions, as well as illusory patterns due to motion signals in line drawings, are due to the statistics of visual computations. The interpretation of image patterns is preceded by a step where image features such as lines, intersections of lines, or local image movement must be derived. However, there are many sources of noise or uncertainty in the formation and processing of images, and they cause problems in the estimation of these features; in particular, they cause bias. As a result, the locations of features are perceived erroneously and the appearance of the patterns is altered. The bias occurs with any visual processing of line features; under average conditions it is not large enough to be noticeable, but illusory patterns are such that the bias is highly pronounced. Thus, the broader message of this paper is that there is a general uncertainty principle which governs the workings of vision systems, and optical illusions are an artifact of this principle.
© 2003 Elsevier Ltd. All rights reserved.

Keywords: Optical illusions; Motion perception; Bias; Estimation processes; Noise

1. Introduction

Optical illusions are fascinating to almost everyone, and recently with a surge in interest in the study of the mind, they have been very much popularized. Some optical illusions, such as the distortion effects in architectural structures of large extent, or the moon illusion, have been known since the antiquity. Some illusions, such as the Müller-Lyer illusion or the Penrose triangle, by now are considered classic and are taught in schools. Many new illusory patterns have been created in the last few years. Some of these are aesthetically pleasing variations of known effects, but others introduced new effects, prominently in motion and lightness.

Scientific work on optical illusions started in the 19th century, when scientists engaged in systematically studying perception, and since then there has been an enduring interest. What is it that has caused this long-standing effort? Clearly, they reveal something about human limitations and by their nature are obscure and thus fascinating. But this has not been the sole reason for scientific interest. For theorists of perception they have been used as test instruments for theory, an effort that originated from the founders of the Gestalt school. An important strategy in finding out how correct perception operates is to observe situations in which mis-perception occurs. Any theory, to be influential, must be consistent with the facts of correct perception but also must be capable of predicting the failures of the perceptual system. In the past the study of illusions has mostly been carried out by psychologists who have tried to gain insight into the principles of perception by carefully altering the stimuli and testing the changes in visual performance. In recent decades they have been joined by scientists of other mind-related fields such as neurology, physiology, philosophy, and the computational sciences, examining the problem from different viewpoints with the use of different tools (Gillam, 1998; Palmer, 1999).

The best known and most studied of all illusions are the geometrical optical illusions. The term is a translation of the German *geometrisch-optische Täuschungen* and has been used for any illusion seen in line drawings.

* Corresponding author.
E-mail address: fer@cfar.umd.edu (C. Fermüller).

It was coined by Oppel (1855) in a paper about the overestimation of an interrupted as compared with an uninterrupted extent, later called the Oppel–Kundt illusion (Kundt, 1863). Some other famous illusions in this class include the Müller-Lyer (Müller-Lyer, 1896), Poggendorff, the Zöllner illusions (Zöllner, 1860), the Fraser spiral (Fraser, 1908), and the contrast effect (Oyama, 1960). The number of illusory patterns that fall in this class is very large, and the perceptual phenomena seem to be quite diverse. This is reflected in a cornucopia of explanations one can find in the literature, most of them concerned with only one, or a small number of illusions (Robinson, 1972).

In this paper we propose a theory that predicts a large number of geometrical optical illusions. This theory states that the statistics of visual computations is the cause or one of the major causes underlying geometrical optical illusions, and also by extension, illusory patterns due to motion signals in line drawings. In a nutshell, when interpreting a pattern, features in the image such as lines, intersections of lines, or local image motion must be derived, that is, they must be estimated from the input data. Because of noise, systematic errors occur in the estimation of the features; in statistical terms we say the estimations are biased. As a result, the locations of features are perceived erroneously and the appearance of the pattern is altered. The bias occurs with any visual processing of features; under average conditions it is not large enough to be noticeable, but illusory patterns are such that the bias is strongly pronounced.

In somewhat more detail, the proposed theory is as follows: our eyes receive as input a sequence of images. The early visual processing apparatus extracts from the images local image measurements. We consider three kinds: the intensity value of image points; small edge elements (edgels); and image motion perpendicular to local edges (normal flow). These image measurements can only be derived within a range of accuracy. In other words, there is noise in the intensity of image points, in the positions and orientations of edge elements, and in the directions and lengths of normal flow vectors. The first interpretation processes estimate local edges from image intensities, intersections of lines from edgels, and local 2D image motion from normal flow measurements. These estimation processes are biased. Thus the perceived positions of edgels are shifted, their directions are tilted, and the intersection of edges and the image movement are estimated wrongly. The local edgel and image motion estimates serve as input to the next higher-level interpretation processes. Long straight lines or general curves are fitted to the edgels and this gives rise to tilted and displaced straight lines and distorted curves as perceived in many illusory patterns. In the case of motion, the local image measurements are combined in segmentation and 3D motion estimation processes, and because of largely different biases in separated re-

gions, this gives rise to the perception of different motions.

The noise originates from a variety of sources. First, there is uncertainty in the images perceived on the retina of an eye because of physical limitations; the lenses cause blurring and there are errors due to quantization and discretization. There is uncertainty in the position since images taken at different times need to be combined, and errors occur in the geometric compensation for location. Even if we view a static pattern our eyes perform movements (Carpenter, 1988) and gather a series of images (either by moving the eyes freely over the pattern or by fixating at some point on it). Next, these noisy images have to be processed to extract edges and their movement. This is done through some form of differentiation process, which also causes noise. Evidence suggests that in the human visual system orientation-selective cells in the cortex respond to edges in different directions (Blasdel, 1992; Hubel & Wiesel, 1961, 1968), and thus errors occur due to quantization. Because of these different sources, there is noise or uncertainty in the image data used in early visual processes, that is, in the image intensity values and their differences in space time, i.e., the spatial and temporal derivatives.

Other authors have discussed uncertainty in measurements before, and argued that optical or neural blur are a cause of some geometrical illusions (Ginsburg, 1975, 1984; Glass, 1970; Grossberg & Mingolla, 1985a, 1985b). Most related to our work are the seminal studies of Morgan and coworkers (Morgan, 1999; Morgan & Casco, 1990; Morgan & Moulden, 1986) and subsequent studies by others (Bulatov, Bertulis, & Mickiene, 1997; Earle & Maskell, 1993) which propose models of band-pass filtering to account for a number of illusions. These studies invoked in intuitive terms the concept of noise, since band-pass filtering also constitutes a statistical model of edge detection in noisy gray-level images. This will be elaborated in the next section. However, the model of band-pass filtering is not powerful enough to explain the estimation of features, different from edges. For this we need to employ point estimation models. Thus, the theme of our study is that band-pass filtering is a special case of a more general principle—namely, uncertainty or noise causes bias in the estimation of image features—and this principle accounts for a large number of geometrical optical illusions that previously have been considered unrelated.

We should stress here, that we use the term *bias* in the statistical sense. In the psychophysical literature the term has been used informally to refer to consistent deviations from the veridical, but not with the meaning of an underlying cause.

Bias in the statistical sense means, we have available noisy measurements and we use a procedure—which we call the estimator—to derive from these measurements a

quantity, let us call it *parameter x*. Any particular small set of measurements leads to a different estimated value for parameter *x*. Assume we perform the estimation of *x* using different sets of measurements many times. The mean of the estimates of *x* (that is, the average of an infinite number of values) is called the *expected value of x*. If the expected value is equal to the true value, the estimate is called *unbiased*, otherwise it is *biased*. In the interpretation of images a significant amount of data is used. Features are extracted by means of estimation processes, for which the mean and the bias are characteristics. This justifies the use of the bias in analysing the perception of features.

The following three sections provide a detailed analysis of the bias in the estimation of the three basic features, the line, the point and the movement of points. (The line and point are the elementary units of the plane, thus they should be the basic features of static images; the movement of points is the elementary unit of sequences of images.) In particular, Section 2 models the estimation of edgels from gray values, Section 3 models the estimation of points as intersection of edgels and Section 4 models the estimation of optic flow from image derivatives. For each model we discuss a number of illusions that are best explained by it. We should emphasize that our goal is to model general computations, but not the specifics of the human vision system. Our vision system probably uses for many interpretation processes different kinds of data. The estimators which are analyzed are linear procedures as these constitute the simplest ways to estimate features in the absence of knowledge about the scene, but we will discuss in Section 5 that other more elaborate estimation processes, assuming the noise parameters are not known, are biased as well. The final Section 6 discusses the relationship to other theories of illusions, and discusses that the bias is a general problem of estimation from noisy data, and thus it affects other visual computations as well.

2. Bias in edge elements

Consider viewing a static scene such as the pattern in Fig. 2. Let the irradiance signal coming from the scene parameterized by image position (x, y) be $I(x, y)$. The image received on the retina can be thought of as a noisy version of the ideal signal. There are two kinds of noise sources to be considered. First, there is noise in the value of the intensity. Assuming this noise is additive, independently and identically distributed, it does not effect the location of edges. Second, there is noise in the spatial location. In other words there is uncertainty in the position—the ideal signal is at location (x, y) in the image, the noisy signal with large probability is at (x, y), but with smaller probability it could also be at location

$(x + \delta x, y + \delta y)$. Let the error in position have a Gaussian probability distribution. The expected value of the image then is obtained by convolving the ideal signal with a Gaussian kernel $g(x, y, \sigma_p)$ with σ_p the standard deviation of the positional noise, that is the expected intensity at an image point amounts to

$$E(I(x, y)) = I(x, y) \star g(x, y, \sigma_p)$$

Gaussian smoothing of static images has been intensively studied in the literature on linear scale space (Koenderink, 1984; Lindeberg, 1994; Witkin, 1983; Yuille & Poggio, 1986), and we can apply the theoretical results derived there.

Edge detection mathematically amounts to localizing the extrema of the first-order derivatives (Canny, 1986) or the zero crossings of second-order derivatives (the Laplacian) (Marr & Hildreth, 1980) of the image intensity function. We are interested in the positions of edges, or the change in positions of edges with variation of the smoothing parameter. Lindeberg (1994) derived formulae for that change in edge position or equivalently the instantaneous velocity of edge points in the direction normal to edges, which he called the drift velocity. We will refer to it as edge displacement.

Consider at every edge point P_0 a local orthonormal coordinate system (u, v) with the v-axis parallel to the spatial gradient direction at P_0 and the u-axis perpendicular to it. If edges are given as the zero crossings of the Laplacian the edge displacement $(\partial_t u, \partial_t v)$ (where t denotes the scale parameter) amounts to

$$(\partial_t u, \partial_t v) = -\frac{\nabla^2(\nabla^2 I)}{2((\nabla^2 I_u)^2 + (\nabla^2 I_v)^2)}(\nabla^2 I_u, \nabla^2 I_v) \tag{1}$$

For a straight edge, where all the directional derivatives in the u-direction are 0, it simplifies to

$$(\partial_t u, \partial_t v) = -\frac{1}{2}\frac{I_{vvvv}}{I_{vvv}}(0, 1) \tag{2}$$

A similar formula is derived in (Lindeberg, 1994) for edges defined as extrema of first-order derivatives. The edge displacement represents the tendency of the movement of edges in scale space. If the scale interval is small the edge displacement in the smoothed image provides a sufficient approximation to the total displacement of the edge, and this is what we will show in later illustrations.

The scale space behavior of straight edges is illustrated in Fig. 1. There are three kinds of edges: edges of type (a) between a dark and a bright region which do not change location under scale space smoothing. Edges of type (b) at the boundaries of a bright line, or bar, in a dark region (or, equivalently, a dark line in a bright region) which drift apart, assuming the smoothing parameter is large enough that the whole bar affects the edges. Edges of type (c) at the boundary of a line of medium brightness next to a bright and a dark region
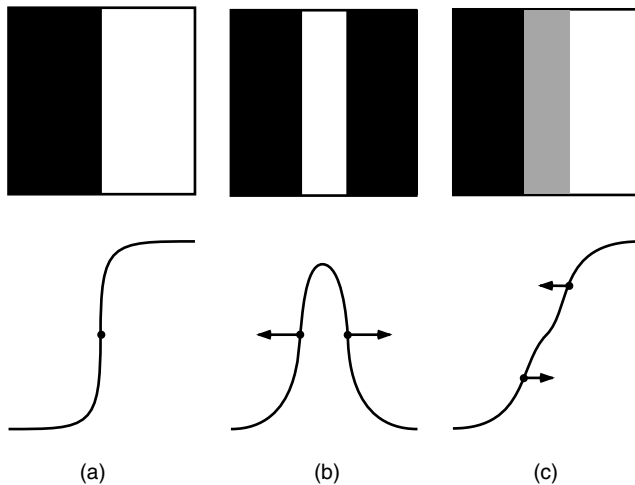
Fig. 1. A schematic description of the behavior of edge movement in scale space. The first row shows the intensity functions of the three different edge configurations, and the second row shows the profiles of the (smoothed) functions with the dots denoting the location of edges: (a) no movement, (b) drifting apart, and (c) getting closer.

Fig. 2. (a) Illusory pattern: "spring" (from Kitaoka, 2003). (b) Small part of the figure to which (c) edge detection, (d) Gaussian smoothing, and (e) smoothing and edge detection have been applied.

which move toward each other. These observations suffice to explain a number of illusions.

The figure in 2a (Kitaoka, 2003) shows a black square grid on a white background with small black squares superimposed. It gives the impression of the straight grid lines being concave and convex curves. The effect can be explained using the above observation. The grid consists of lines (or bars), and the effect of smoothing on the bars is to drift the two edges (of type (b)) apart. At the locations, however, where a square is aligned with the grid, there is only one edge (type (a)), and this edge stays in place. The net effect of smoothing is that edges of grid lines are no longer straight as is illustrated. Fig. 2b shows a small part of the figure magnified. The black squares in the center of the grid all have been removed for clarity, as they do not notably affect the illusory perception. Fig. 2c shows the results of edge detection on the raw image using the Laplacian of a Gaussian (LoG). Fig. 2d shows the smoothed image which results from filtering with a Gaussian with standard deviation 5/4 times the width of the bars and Fig. 2e shows the result of edge detection on the smoothed image using a LoG. (This is clearly the same as performing edge detection on the raw image with a LoG of larger standard deviation.)

Fig. 3a shows an even more impressive pattern from (Kitaoka, 2003): a black and white checkerboard with little white squares superimposed in corners of the black tiles close to the edges, which gives the impression of wavy lines. In this pattern, next to the white squares short bars are created—a white area (from a little square) next to a black bar (from a black checkerboard tile) next to a white area (from a white checkerboard tile). The edges of these bars (edges of type (b)) drift
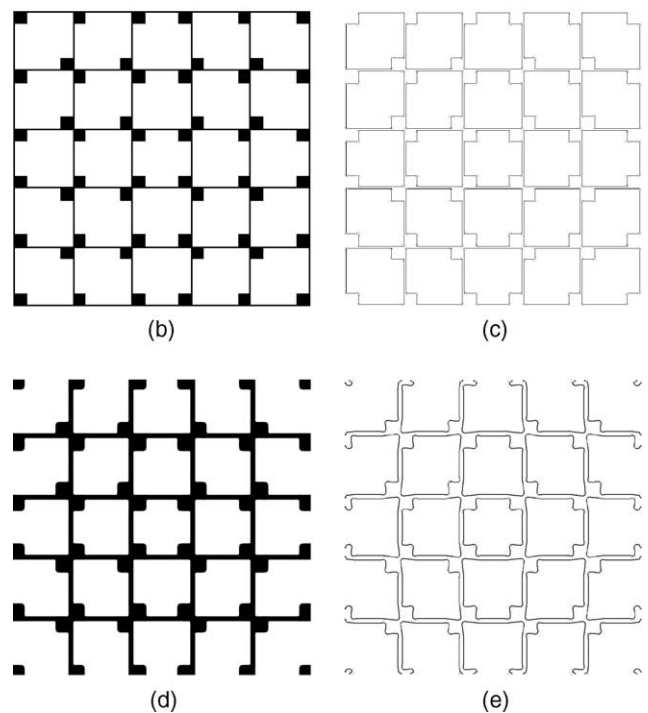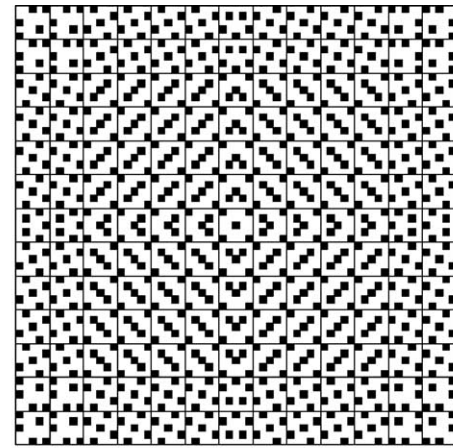
apart under smoothing. The other edges (of type (a))—between the black and white tiles of the checkerboard—stay in place. As a result the edges near the locations of the white squares appear bumped outward toward the white checkerboard tiles. This is illustrated in Fig. 3b which shows the combined effect of smoothing and edge detection for a part of the pattern. Fig. 3c and d zoom in on the edge movement.

Another illusory pattern in this category is the "café wall" illusion shown in Fig. 4a. It consists of a black and white checkerboard pattern with alternate rows shifted one half-cycle and with thin mortar lines, mid-way in luminance between the black and white squares,
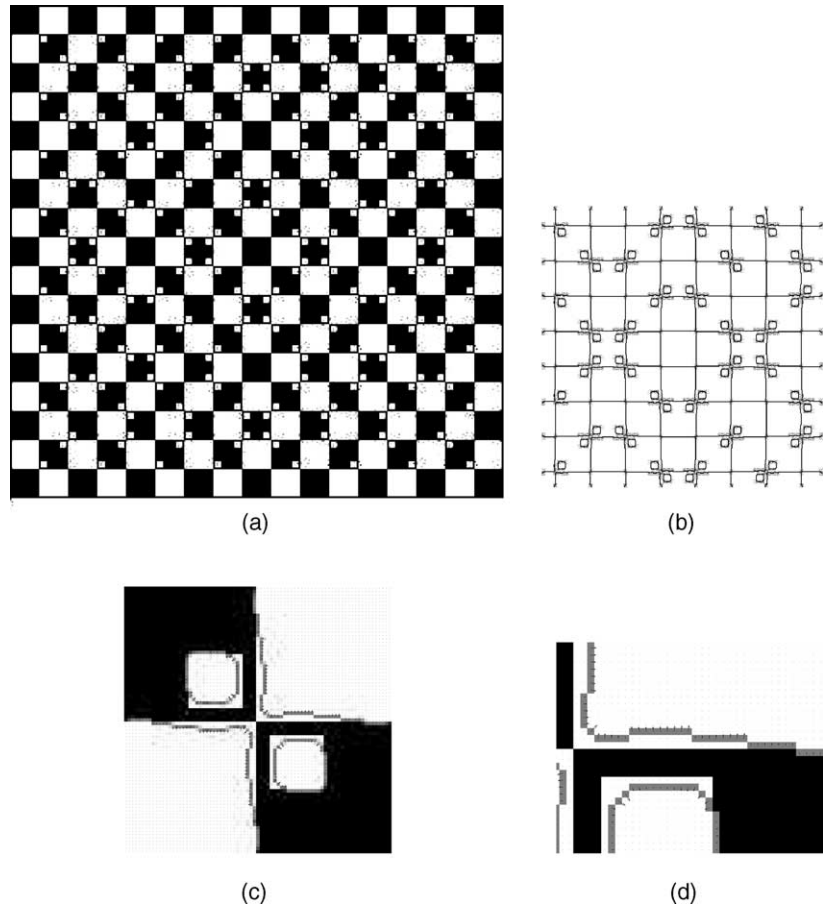
Fig. 3. (a) Illusory pattern: "waves" (from Kitaoka, 2003). (b) The result of smoothing and edge detection on a part of the pattern. (c, d) The drift velocity at edges in the smoothed image logarithmically scaled for parts of the pattern.
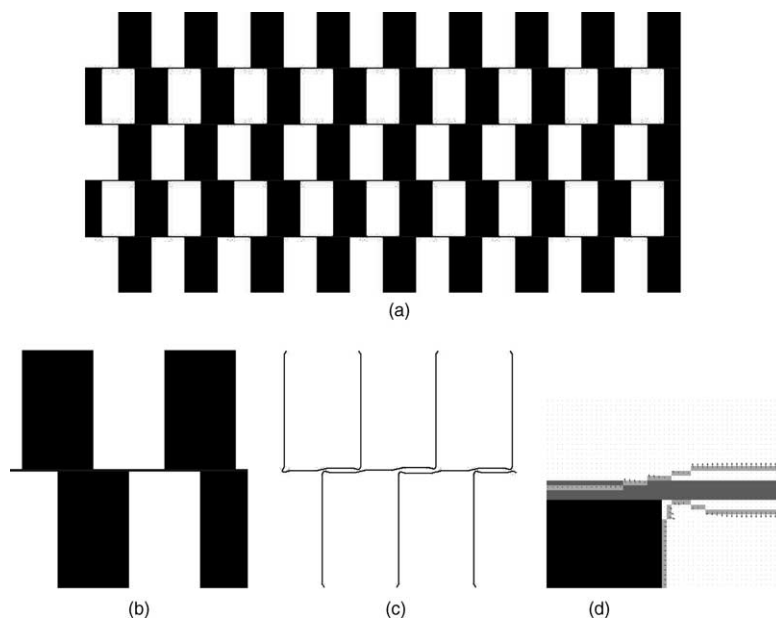

Fig. 4. (a) Café wall illusion. (b) Small part of the figure. (c) Result of smoothing and edge detection. (d) Zoom-in on the edge movement.

separating the rows. At the locations where a mortar line borders both a dark tile and a bright tile the two edges move toward each other, and for thin lines it takes a relatively small amount of smoothing for the two edges to merge into one. Where the mortar line is between two bright regions or where it is between two dark regions the edges move away from each other. The results of smoothing and edge detection are shown in Fig. 4c for a small part of the pattern as in Fig. 4b. The movement of edges under scale space smoothing is illustrated in Fig. 4d.

We can counteract the effect of bias by introducing additional elements as shown in Fig. 5a; the additional white and black squares put in the corners of the tiles greatly reduce the illusory effect. As illustrated in Fig. 5c the inserted squares partly compensate for the drifting of edges in opposite directions. As a result slightly wavy edgels are obtained; but the "waviness" is too weak to be perceived (low amplitude, high frequency).

A full account of the perception of lines in the above illusions requires additional explanation. The lines are derived in two (or more) processing stages. In the first stage local edge elements are computed which are tilted because of bias. The second stage consists of the integration of these local elements into longer lines. Our hypothesis is that this integration is computationally an approximation of the longer lines using as input the positions and orientations of the edge elements. If the linking of edge elements is carried out this way tilted lines will be computed in the café wall pattern and curved lines will be derived in the pattern "waves." Line fitting possibly could be realized as smoothing in orientation space (Morgan & Hoptopf, 1989) implemented in a multi-resolution architecture. At every resolution the average of the directions of neighboring elements is computed, and all the computations are local. In the case of general curves increasingly larger segments of increasingly higher complexity could be fitted to smaller segments; computationally it amounts to a form of spline fitting.

An integration process of this form also explains one of the most forceful of all illusions, the Fraser spiral pattern, which consists of circles made of black and white elements which together form something rather like a twisted cord, on a checkerboard background. The twisted cord gives the perception of being spiral-shaped, rather than a set of circles. The individual black and white elements which make up the cord are sections of spirals, thus also the edges at the borders of the black and white lines are along theses directions and the approximation process will fit spirals to them.

The concept of blurring has been invoked before by several authors as an explanation of some geometrical optical illusions (Chiang, 1968; Ginsburg, 1984; Glass,
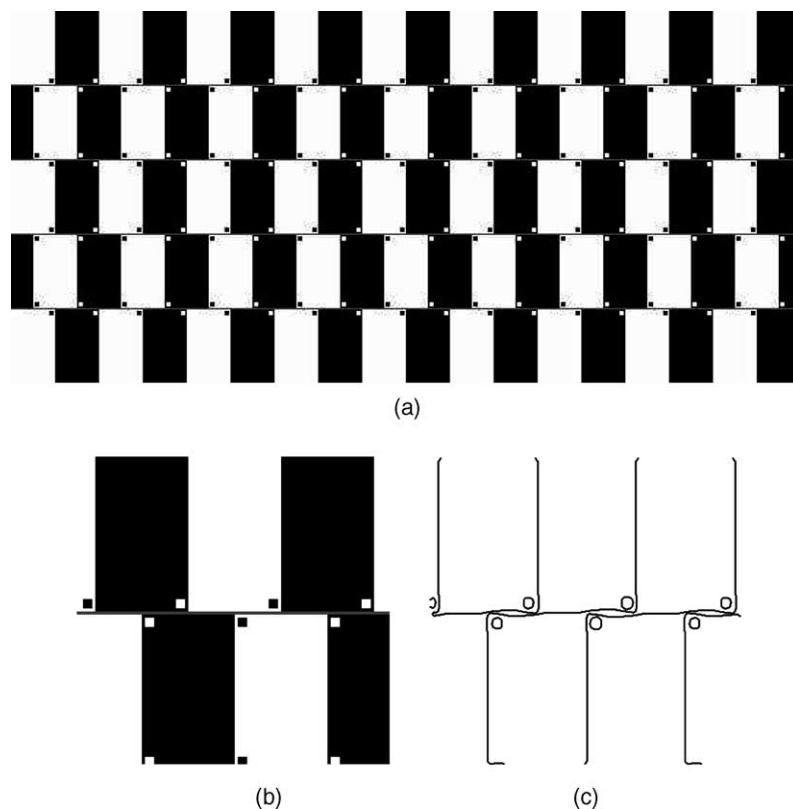

(a)

(b)　　　　　　　　　　(c)

Fig. 5. Modified café wall pattern. The additional black and white squares change the edges in the filtered image, which counteracts the illusory effect.

1970). In particular, the café wall illusion has been explained by means of band-pass filtering in the visual system (Earle & Maskell, 1993; Morgan & Moulden, 1986). Fraser (1908) already related the effect in the Münsterberg illusion to his own twisted cord phenomenon. Morgan and Moulden (1986) showed that a pattern like the twisted cords is revealed in the mortar lines if the café wall figure is processed with a band-pass spatial frequency filter (smoothed Laplacians and difference of Gaussians). The cords consist of the peaks and troughs (maxima and minima) in the filtered image. We referred to the zero crossings. But essentially our explanation for the cause in the tilt in the edgels in the café wall illusion is not different from the one in (Morgan & Moulden, 1986). This is, because the effect of noise in gray values on edge detection is computationally like band-pass filtering.

Within our framework the interpretation of band-pass filtering is different. We do not say that edge detection is carried out by band-pass filtering, although this may be the case. We say that the expected image (that is the image estimated from noisy input) is like a
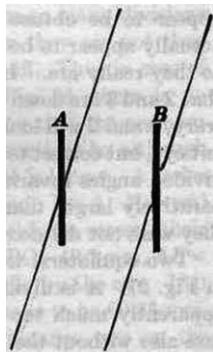

Fig. 6. The fine line as shown in *A* appears to be bent in the vicinity of the broader black line, as indicated in exaggeration in *B* (from Helmholtz, 1962, Chap. 28).
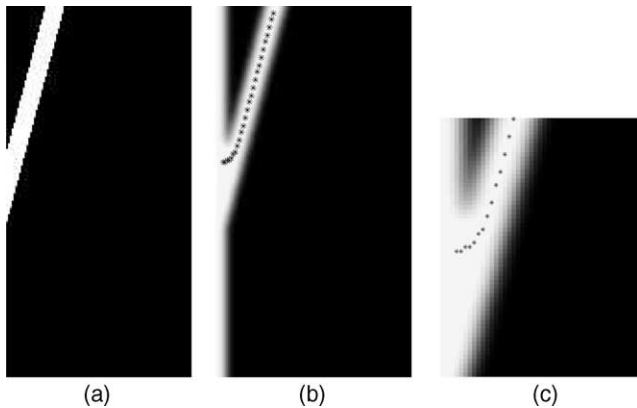

Fig. 7. (a) A line intersecting a bar at an angle of 15°. (b) The image has been smoothed and the maxima of the gray-level function have been detected and marked with stars. (c) Magnification of intersection area.

smoothed image, and edges in smoothed images are biased. In other words, their location does not correspond to the location in the perfect image. It does not matter what the source of the noise is, and it does not matter how edges are computed, with Laplacians or as maxima of first-order derivatives.

The perceptual effect at intersecting lines is illustrated in Fig. 6. It can be shown with the model introduced in this section that the intersection point of two lines which intersect at an acute angle is displaced. The effect is obtained by smoothing the image and then detecting edges using non-maximum suppression (see Fig. 7). A more detailed analysis of the behavior of intersecting lines is the topic of the next section.

3. Bias in intersection points

There is a large group of illusions in which lines intersecting at angles, particularly acute angles, are a decisive factor in the illusion. Wundt (1898) drew attention to this; acute angles are overestimated, and obtuse angles are slightly underestimated (although regarding the latter there has been controversy). We predict that these phenomena are due to the bias in the estimation of the intersection point.

We adopt in this section a slightly different noise model, with the noise being defined directly on the edge elements. Noise in gray-level values results in noise in the estimated edge elements, but also the differentiation process creates noise. The problem of finding the intersection points then can be formulated as solving a system of linear equations. This allows for a clean analysis of the influences of the different parameters on the solutions, and thus provides a powerful predictive model.

Consider the input to be edge elements, parameterized by the image gradient (a vector in the direction normal to the edge) (I_x, I_y) and the position of the center of the edge element (x_0, y_0). The edge elements are noisy (see Fig. 8a). There is noise in the position (which as will be shown, however, does not contribute to the bias) and there is noise in the orientation. To obtain the intersection of straight lines, imagine a line through every edge element, and compute the point closest to all the lines (Fig. 8b).

In algebraic terms: consider additive, independently and identically distributed (i.i.d.) zero-mean noise in the parameters of the edgels. In the sequel unprimed letters are used to denote estimates, primed letters to denote actual values, and δ's to denote errors, where $I_x = I'_x + \delta I_x$, $I_y = I'_y + \delta I_y$, $x_0 = x'_0 + \delta x_0$ and $y_0 = y'_0 + \delta y_0$.

For every point (x, y) on the lines the following equation holds:

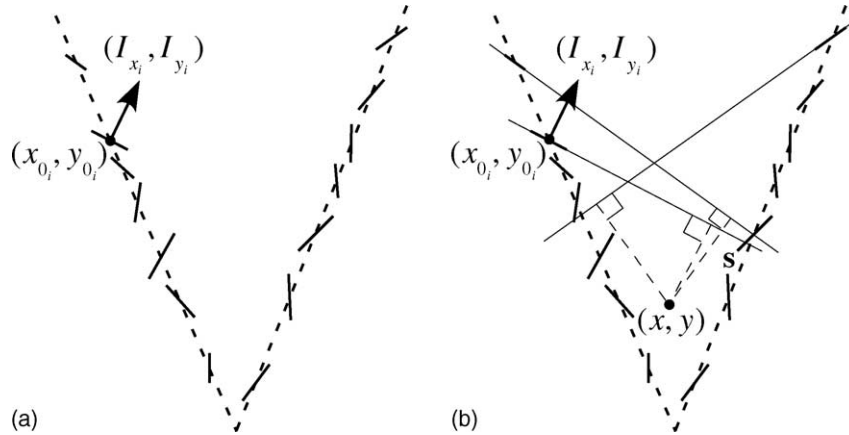$$I'_x x + I'_y y = I'_x x'_0 + I'_y y'_0 \tag{3}$$

Fig. 8. (a) The inputs are edge elements parameterized by the position of their centers (x_{0_i}, y_{0_i}) and the image gradient (I_{x_i}, I_{y_i}). (b) The intersection of straight lines is estimated as the point closest to all the "imaginary" lines passing through the edge elements.

This equation is approximated by the measurements. Let n be the number of edge elements. Each edgel measurement i defines a line given by the equation

$$I_{x_i}x + I_{y_i}y = I_{x_i}x_{0_i} + I_{y_i}y_{0_i} \qquad (4)$$

and we obtain a system of equations which is represented in matrix form as

$$I_s\vec{x} = \vec{c}$$

Here I_s is the $n \times 2$ matrix which incorporates the data in the I_{x_i} and I_{y_i}, and $\vec{c}$ is the n-dimensional vector with components $I_{x_i}x_{0_i} + I_{y_i}y_{0_i}$. The vector $\vec{x}$ denotes the intersection point whose components are x and y. The solution to the intersection point using standard least square (LS) estimation is given by

$$\vec{x} = (I_s^{\mathrm{T}}I_s)^{-1}I_s^{\mathrm{T}}\vec{c} \qquad (5)$$

where superscript T denotes the transpose of a matrix. It is well known that the LS solution to a linear system of the form $A\vec{x} = \vec{b}$ with errors in the measurement matrix A is biased (Fuller, 1987). The statistics for the case of i.i.d. noise in the parameters of A and $\vec{b}$ can be looked up in books. Our case is slightly different, as $\vec{b}$ is the product of terms in A and two other noisy terms.

To simplify the analysis, let the variance of the noise in the spatial derivatives in the x- and y-directions be the same, let it be σ_s^2. Assuming the expected values of higher- (than second) order terms to be negligible, the expected value of $\vec{x}$ is found by developing (5) into a second-order Taylor expansion at zero noise (as derived in Appendix A). It converges in probability to

$$\lim_{n\to\infty} E(\vec{x}) = \vec{x}' + \sigma_s^2 \left(\lim_{n\to\infty} \left(\frac{1}{n}M' \right) \right)^{-1} (\vec{x}_0' - \vec{x}') \qquad (6)$$

where

$$M' = I_s'^{\mathrm{T}}I_s' = \begin{bmatrix} \sum_{i=1}^{n} I_{x_i}'^2 & \sum_{i=1}^{n} I_{x_i}'I_{y_i}' \\ \sum_{i=1}^{n} I_{x_i}'I_{y_i}' & \sum_{i=1}^{n} I_{y_i}'^2 \end{bmatrix}$$

$\vec{x}'$ is the actual intersection point, $\vec{x}_0' = \begin{bmatrix} \frac{1}{n}\sum_{i=1}^{n} x_{0_i}' \\ \frac{1}{n}\sum_{i=1}^{n} y_{0_i}' \end{bmatrix}$ is the mean of the $\vec{x}_{0_i}'$, and n denotes the number of edge elements.

Using (6) allows for an interpretation of the bias. The estimated intersection point is shifted by a term which is proportional to the product of matrix M'^{-1} and the difference vector $(\vec{x}_0' - \vec{x}')$. Vector $(\vec{x}_0' - \vec{x}')$ extends from the actual intersection point to the mean position of the edge elements. Thus it is the mass center of the edgels that determines this vector. M' depends only on the spatial gradient distribution. As a real symmetric matrix its two eigenvectors are orthogonal, and the direction of the eigenvector of the larger eigenvalue is dominated by the major direction of gradient measurements. M'^{-1} has the same eigenvectors as M' and inverse eigenvalues and therefore, the influence of M'^{-1} is strongest in the direction of the smallest eigenvalue of M'. Consider the case of two intersecting lines, and thus two gradient directions; the effect of M'^{-1} is more bias in the direction of fewer image gradients and less bias in the direction of more gradients. This means more displacement of the intersection point in the direction perpendicular to the line with fewer edge elements.

Fig. 9a shows the most common version of the Poggendorff illusion (as described by Zöllner, 1860). The upper-left portion of the interrupted, tilted straight line in this figure is apparently not the continuation of the lower portion on the right, but is too high. Another version of this illusion is shown in Fig. 9b. Here it appears that the middle portion of the inclined (interrupted) line is not in the same direction as the two outer patterns, but is turned clockwise with respect to them.

Referring to Fig. 9a, the intersection point of the left vertical with the upper tilted line is moved up and to the left, and the intersection point of the right vertical with the lower tilted line is moved down and to the right. This should be a contributing factor in the illusion. However, there are most likely other causes to this illusion, maybe
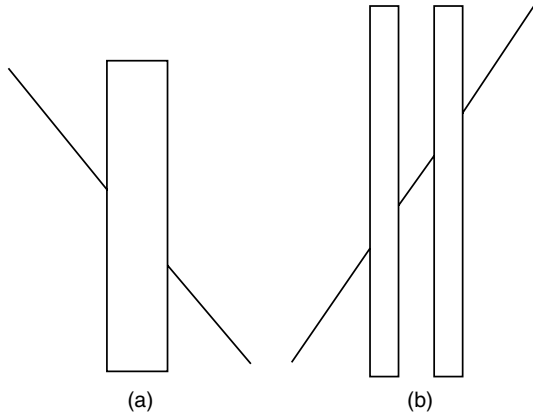
Fig. 9. Poggendorff illusion.

biases in higher-level processes which analyze larger regions of the image to compare the different line segments.

From parametric studies it is known that the illusory effect decreases with an increase in the acute angle (Cameron & Steele, 1905; Wagner, 1969). Our model predicts this, as can be deduced from Fig. 10. For a tilted line intersecting a vertical line at its mid-point in an angle ϕ, we plotted the value of the bias in x- and y-direction as a function of the angle ϕ. As can be seen, as the angle increases, the bias in both components decreases.

Fig. 11 shows two versions of the well-known Zöllner illusion (Zöllner, 1860). The vertical bands in Fig. 11a and the diagonal lines in Fig. 11b (Hering, 1861) are all parallel, but they look convergent or divergent. Our theory predicts that in these patterns the biases in the intersection points of the long lines (or edges of bands) with the short line segments cause the edges along the long lines between intersection points to be tilted. The

estimation is illustrated in Fig. 12 for a pattern as in Fig. 11a with 45° between the vertical and the tilted bars. In a second computational step, long lines are computed as an approximation to these small edge pieces. If, as discussed in the previous section, the positions and orientations of the line elements are used in the approximation, tilted lines or bars will be computed which are in the same direction as perceived by the visual system.

In experiments with this illusion it has also been found that the effect decreases with an increasingly acute angle between the main line and the obliques, which can be explained as before using Fig. 10b and c (or, similarly, Fig. 15). The value where the maximum occurs varies among different studies. It is somewhere between 10° and 30°; below that, some counteracting effects seem to take place (Morinaga, 1933; Wallace & Crampin, 1969).

Other parametric studies have been conducted on the effect of altering the orientations of the Poggendorff and Zöllner figures. The Poggendorff illusion was found to be strongest with the parallel lines vertical or horizontal (Green & Hoyle, 1964; Leibowitz & Toffey, 1966). The Zöllner illusion, on the other hand, was found to be maximal when the judged lines were at 45° (Judd & Courten, 1905; Morinaga, 1933), as in Fig. 11b.

The term "spatial norms" is used to refer to the vertical and horizontal directions: we generally see better in these orientations (Howard & Templeton, 1966). There also is evidence from brain imaging techniques for more activity in early visual areas (V1) for horizontal and vertical than for oblique orientations (Furmanski & Engel, 2000). Based on these findings we can assume there is more data for horizontal and vertical lines, that is, more edge elements are estimated in these and nearby directions. This in turn amounts to higher accuracy in
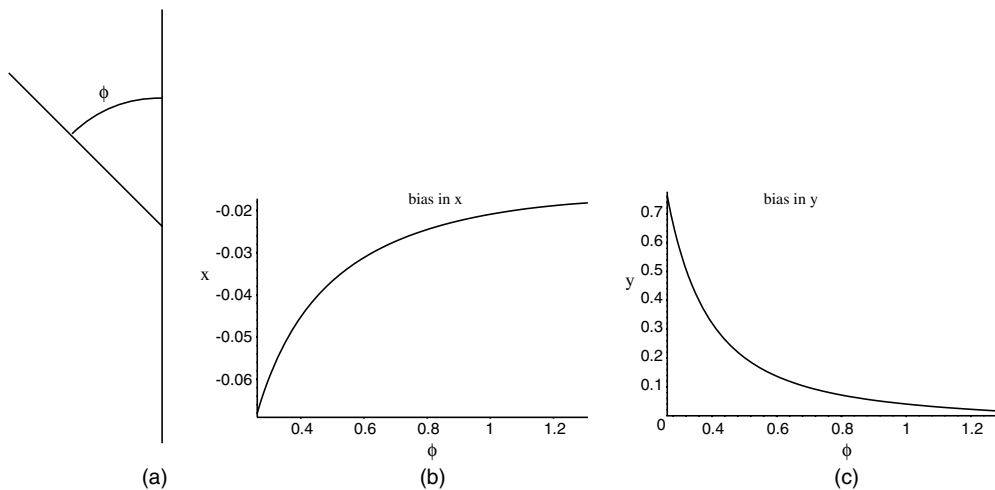

Fig. 10. (a) A tilted line intersects a vertical line at its mid-point at an angle ϕ. The data used was as follows: the tilted line had length 1, the vertical had length 2, and the edge elements with noise in the spatial derivatives of $\sigma = 0.08$ were distributed at equal distances. (b) Bias perpendicular to the vertical and (c) bias parallel to the vertical.
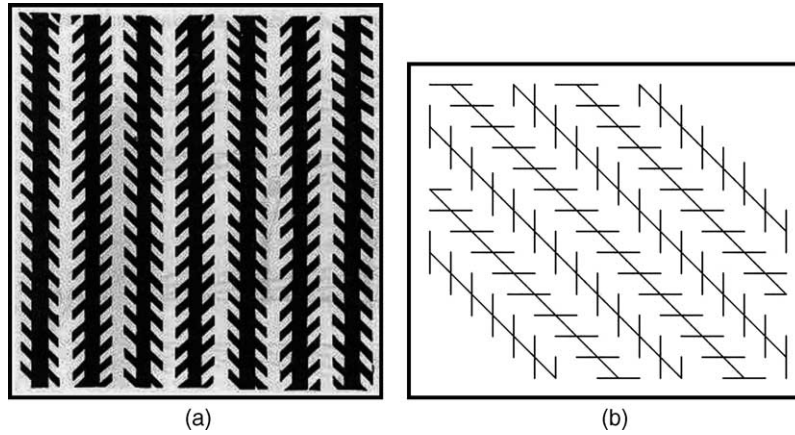
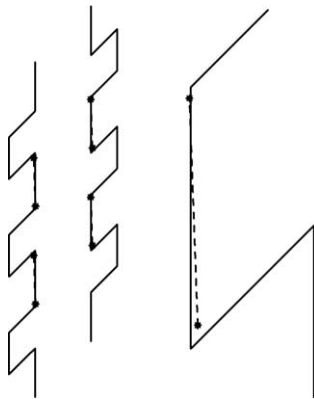Fig. 11. (a) Zöllner pattern. (b) Hering's version of the Zöllner pattern gives increased illusory effect.

Fig. 12. The estimation of edges in the Zöllner pattern: the edge elements were found by connecting two consecutive intersection points, resulting from the intersection of edges of two consecutive tilted bars with the edge of the vertical bar (one in an obtuse and one in an acute angle). As input we used edge elements uniformly distributed on the vertical and on the tilted lines with 1.5 times more elements on the vertical.

the estimation of quantities in this direction. Intuitively, in a direction where there are more estimates there is a larger signal to noise ratio, and this results in greater accuracy in this direction.

Expressed in our formalism of Eq. (6), this takes the following form. The effect of the gradient distribution on the bias is strongest in the direction of the eigenvector corresponding to the smaller eigenvalue of M' and weakest in the orthogonal direction. Changing the ratio of measurements (edgels) along the different lines changes the bias. Fig. 13 illustrates, for the case of a vertical line intersecting an oblique line at an angle of 30°, the bias in the x- and y-directions as a function of the ratio of edge elements. It can be seen that as the ratio of vertical to oblique elements increases, the bias in the x-direction decreases and the bias in the y-direction increases. The Poggendorff illusion is stronger when the parallel lines are vertical or horizontal, because in this case the bias parallel to the lines (along the y-axis in the plot) is larger, and the Zöllner illusion is stronger when the small lines are horizontal and vertical and the main lines are tilted, as in this case the bias perpendicular to the main lines (along the x-axis in the plot) is larger.

Many other well-known illusions can be explained on the basis of biased line intersection. Examples are the Orbison figures (Orbison, 1939), Wundt's figure (Wundt, 1898), and the patterns of Hering (1861) and Lukiesh (1922). In these patterns geometrical entities such as straight lines, circles, triangles or squares are superimposed on differently tilted lines, and they appear
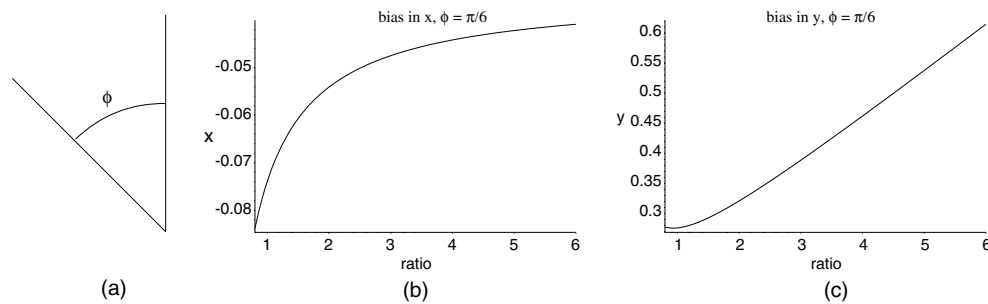

Fig. 13. (a) A vertical line intersecting a tilted line at an angle $\phi = \pi/6$ (the length of the vertical and the tilted line is one unit and $\sigma = 0.06$). (b) Bias perpendicular to the vertical as a function of the ratio of edge elements on the vertical and tilted lines. (c) Bias parallel to the vertical.

to be distorted. This distortion can be accounted for by the erroneous estimation of the tilt in the line elements between intersection points and the subsequent fitting of curves to these line elements.

Fig. 14 illustrates the estimation of the curve in the Luckiesh pattern. Each line has two edges, and we computed the intersection between any background edge and circle edge (using configurations such as those in Fig. 13a). This provided for every intersection of the circle with a straight line four intersection points, two corresponding to the inner edges of the circle and two to the outer ones. Arcs on the circle between two consecutive background lines were approximated by straight lines. (The ratio of elements between the circle and the background edge was 2:1 (resulting in a configuration similar to that of Fig. 15 with the arc corresponding to the vertical.)—Note, other ratios give qualitatively similar results.) Consecutive intersection points—one originating from an obtuse and one from an acute angle—were connected with straight line segments. Bezier splines were then fitted to the outer line segments. This resulted in a curve like the one we perceive, with the circle being bulbed out on the upper and lower left and bulbed in on the upper and lower right.

Next, let us look at the erroneous estimation of angles. Assuming that the erroneously estimated intersection point has a distorting effect on the arms (Wallace, 1969), the bias discussed for the above illusions will result in the overestimation of acute angles. The underestimation of obtuse angles can be explained if we assume an unequal amount of edgel data on the two arcs. Fig. 15 illustrates the bias for acute and obtuse angles for the case of more edge elements on the vertical than on the tilted line. The bias in the x-direction changes sign and the bias in the y-direction increases (with increasing angle) for obtuse angles, and this results in a small underestimation of obtuse angles.

We used the intersection point as main criterion to explain the illusions discussed in this section. But very likely many of these illusions are due to the estimation of multiple features. In particular, for illusions involving many small line segments, such as the Zöllner pattern, estimation of edges and estimation of intersection points would have very similar results.

Illusions of intersecting lines have been intensely studied, and there are also models that employ in some form the concept of noise. Morgan and Casco (1990) propose as explanation of the Zöllner and Judd illusion
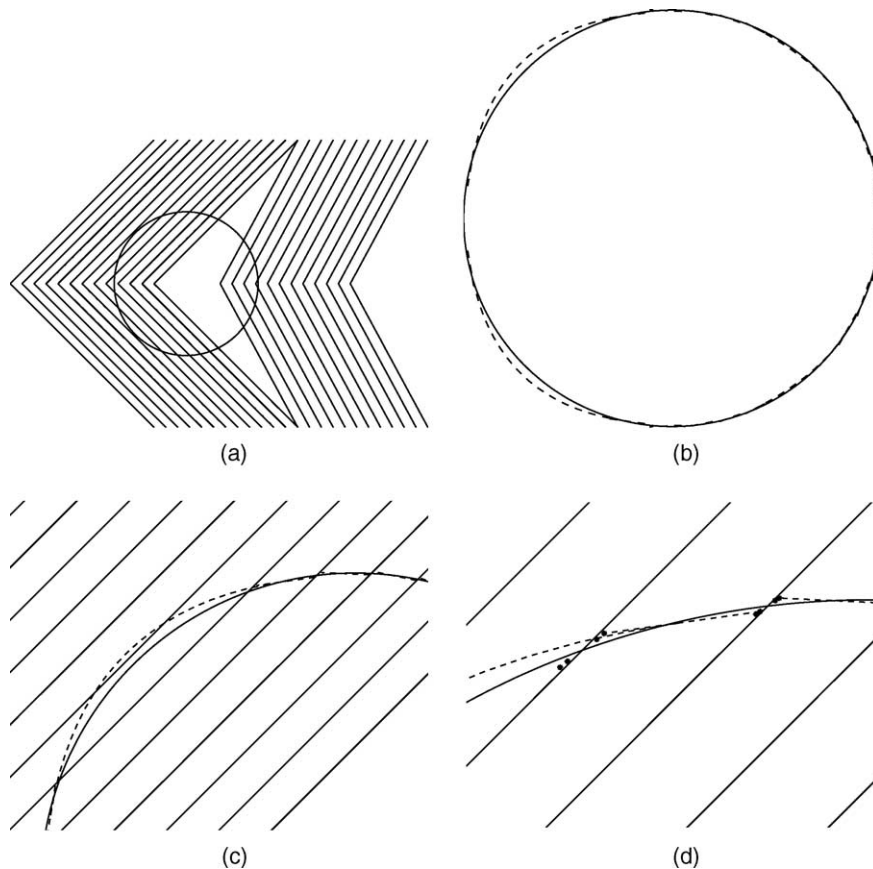

Fig. 14. Estimation of Luckiesh pattern: (a) the pattern—a circle superimposed on a background of differently arranged parallel lines, (b) fitting of arcs to the circle, (c) magnified upper-left part of pattern with fitted arcs superimposed, and (d) intersection points and fitting of segments to outer intersections.
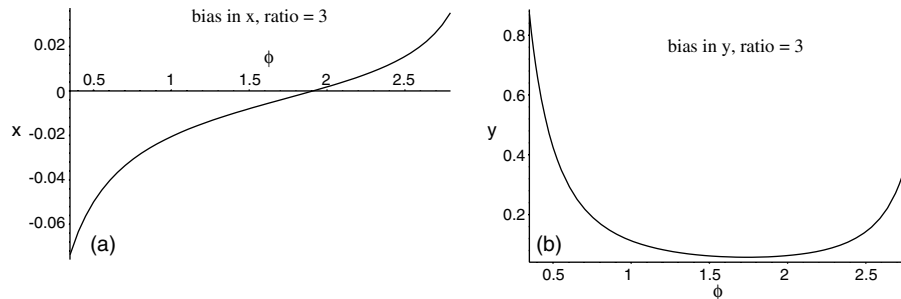
Fig. 15. A vertical line and a tilted line of length 1 intersecting at an angle ϕ; the ratio of vertical to tilted edge elements is 3:1; $\sigma = 0.06$. (a) Bias perpendicular to the vertical. (b) Bias parallel to the vertical.

band-pass filtering followed by feature extraction in second stage filters. The features are the extrema in the band-pass filtered image, which correspond to the intersection points. Morgan (1999) studied the Poggendorff illusion and suggests smoothing in second stage filters as the main cause.

4. Bias in motion

When processing image sequences some representation of image motion must be derived as a first stage. It is believed that the human visual system computes two-dimensional image measurements which correspond to velocity measurements of image patterns, called optical flow. The resulting field of measurements, the optical flow field, represents an approximation to the projection of the field of motion vectors of 3D scene points on the image.

Optical flow is derived in a two-stage process. In a first stage the velocity components perpendicular to linear features are computed from local image measurements. This one-dimensional velocity component is referred to as "normal flow" and the ambiguity in the velocity component parallel to the edge is referred to as the "aperture problem." In a second stage the optical flow is estimated by combining, in a small region of the image, normal flow measurements from features in different directions, but this estimate is biased.

We consider a gradient-based approach to deriving the normal flow. The basic assumption is that image gray level does not change over a small time interval. Denoting the spatial derivatives of the image gray level $I(x, y, t)$ by I_x, I_y, the temporal derivative by I_t, and the velocity of an image point in the x- and y-directions by $\vec{u} = (u, v)$, the following constraint is obtained:

$$I_x u + I_y v + I_t = 0 \tag{7}$$

This equation, called the optical flow constraint equation, defines the component of the flow in the direction of the gradient (Horn, 1986). We assume the optical flow to be constant within a region. Each of the n measurements in the region provides an equation of the form (7) and thus we obtain the over-determined system of equations

$$I_s \vec{u} + \vec{I}_t = 0 \tag{8}$$

where I_s denotes, as before, the matrix of spatial gradients (I_{x_i}, I_{y_i}), $\vec{I}_t$ the vector of temporal derivatives, and $\vec{u} = (u, v)$ the optical flow. The least squares solution to (8) is given by

$$\vec{u} = -(I_s^t I_s)^{-1} I_s^\mathrm{T} \vec{I}_t \tag{9}$$

As a noise model we consider zero-mean i.i.d. noise in the spatial and temporal derivatives, and for simplicity, equal variance σ_s^2 for the noise in the spatial derivatives.

The statistics of (9) are well understood, as these are the classical linear equations. The expected value of the flow, using a second-order Taylor expansion, is derived in Appendix A; it converges to

$$\lim_{n \to \infty} E(\vec{u}) = \vec{u}' - \sigma_s^2 \left(\lim_{n \to \infty} \left(\frac{1}{n} M' \right) \right)^{-1} \vec{u}' \tag{10}$$

where, as before, the actual values are denoted by primes.

Eq. (10) is very similar to Eq. (6) and the interpretation given there applies here as well. It shows that the bias depends on the gradient distribution (that is, the texture) in the region. Large biases are due to large variance, ill-conditioned M, or an $\vec{u}$ which is close to the eigenvector of the smallest eigenvalue of M. The estimated flow is always underestimated in length, and it is closer in direction to the direction of the majority of normal flow vectors than the veridical.

Fig. 16 shows a variant of a pattern created by Ouchi (1977). The pattern consists of two rectangular checkerboard patterns oriented in orthogonal directions—a background orientation surrounding an inner ring. Small retinal motions, or slight movements of the paper, cause a segmentation of the inset pattern, and motion of the inset relative to the surround. This illusion has been discussed in detail in (Fermüller, Pless, & Aloimonos, 2000). We will thus only give a short description here.
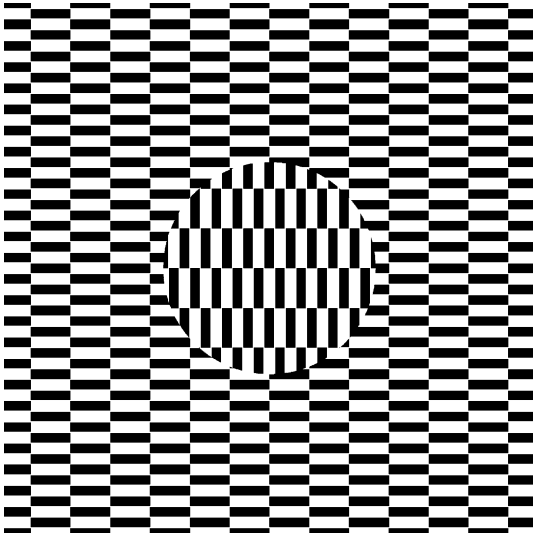
Fig. 16. A pattern similar to the one by Ouchi.

Fig. 18. If fixating on the center and moving the paper along the line of sight, the inner circle appears to rotate.

The tiles used to make up the pattern are longer than they are wide leading to a gradient distribution in a small region with many more normal flow measurements in one direction than the other. Since the tiles in the two regions of the figure have different orientations, the estimated regional optical flow vectors are different. The difference between the bias in the inset and the bias in the surrounding region is interpreted as motion of the ring. An illustration is given in Fig. 17 for the case of motion along the first meridian (to the right and up). In addition to computing flow, the visual system also performs segmentation, which is why a clear relative motion of the inset is seen.

Another impressive illusory pattern from Pinna and Brelstaff (2000) is shown in Fig. 18. If fixating on the center and moving the page (or the head) along the optical axis back and forth the inner circle appears to rotate—clockwise with a motion of the paper away from the eyes. For a backward motion of the paper the motion vectors are along lines through the image center, pointing away from the center. The normal flow vectors
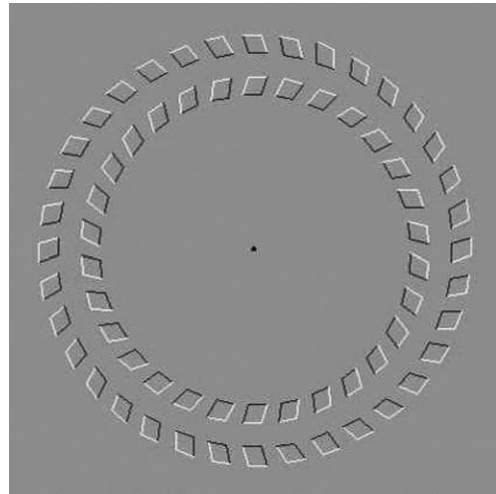
are perpendicular to the edges of the parallelograms. Thus the estimated flow vectors are biased in the clockwise direction in the outer ring and in the counterclockwise direction in the inner ring, as shown in Fig. 19. The difference between the inner and outer vectors (along a line through the center) is tangential to the circles, and this explains the perceived rotational movement. In a similar way one can explain the perception of a spiral movement when rotating the pattern around an axis through the center and perpendicular to the paper. The illusory effect is very much decreased by slightly changing the pattern as in Fig. 20. In this figure the inserted diagonal lines make the local gradient distribution in the inner and outer parallelograms about the same, and thus there is no significant difference in bias which could cause the perception of motion.

To be more rigorous, the estimation is somewhat more elaborate. The vision system not only computes
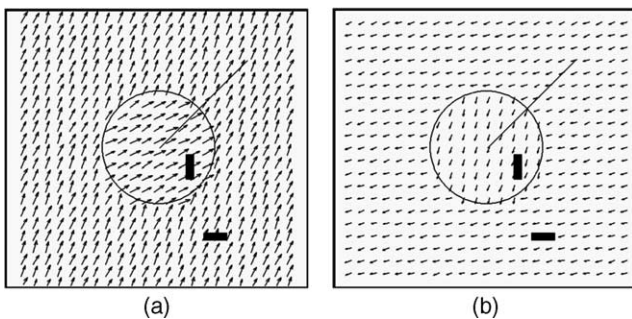

Fig. 17. (a) The optical flow field. (b) The error vector field—the difference between the estimated and the veridical motion. The line from the center is the direction of the veridical motion.
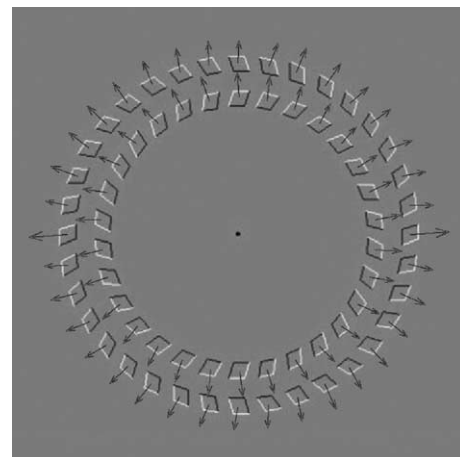

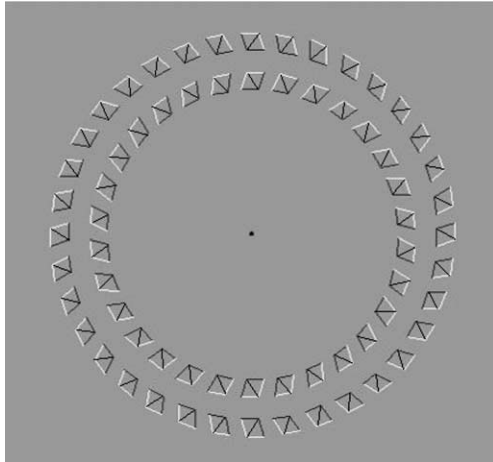Fig. 19. Flow field computed from Fig. 18.

Fig. 20. Modification of Fig. 18 reduces the illusory motion.

Fig. 21. The eye motion gives rise to flow $\mathbf{u}'$ and normal flow vectors $\mathbf{n}_1$ and $\mathbf{n}_2$. The estimated flow, $\mathbf{u}$, has a positive y-component, which causes illusory motion upward in the band.

normal flow and flow on the basis of the raw image. It also smoothes, or blurs, the image and computes normal flow and flow from the blurred image. That is, the vision system utilizes flow at different levels of resolution. For the pattern here the flow vectors at different resolutions are in the same orientation, thus there will be no difference whether the system used multiple resolutions or not. However, one may modify the pattern by changing the black and white in the edges, thus creating bias in one direction at high resolution and bias in the other direction at low resolution, and this way reduce the illusion (as in Fig. 6 in Pinna & Brelstaff, 2000).

Helmholtz (1962) describes an experiment with the Zöllner pattern which causes illusory motion. When the point of a needle is made to traverse Zöllner's pattern (Fig. 11a) horizontally from right to left, its motion being followed by the eye, a perception of motion in the bands occurs. The first, third, fifth and seventh black bands ascend, while the second, fourth, and sixth descend; it is just the opposite when the direction of the motion is reversed.

The bias predicts this effect as follows: a motion of the eyes from right to left gives rise to optical flow from left to right. For each band there are two different gradient directions, i.e., there are two different normal flow components in each neighborhood. For the odd bands the two normal flow components are in the direction of the flow and diagonally to the right and up. Thus the estimated flow makes a positive angle with the actual flow (that is, it has a positive y-component), and this component along the y-axis is perceived as upward motion of the bands (see Fig. 21). For even bands the estimated flow is biased downward, causing the perception of descent of the bands. Similarly, if the motion of the eye is reversed the estimated flow has a negative y-component in the odd bands and a positive y-component in the even bands, leading to a reversal in the perceived motions of the bands.
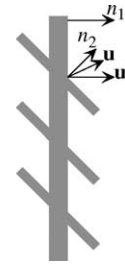
We need to clarify here two issues. First, the simple model of constant flow in a neighborhood in general is not adequate to model image motion. We have used this model here for the purpose of a simple analysis. This model is sufficient only for fronto-parallel scenes and translational motions parallel to the image plane. In the general case we have to segment the flow field at the discontinuities and within coherent regions allow for spatially smooth variation of the flow (Hildreth, 1983; Horn & Schunk, 1981). Smoothness may be modeled by describing the flow as a smooth function of position, or by minimizing, in addition to the deviation from the flow constraint equation, a function of the spatial derivatives of the flow. But the principle of bias is still there (Fermüller, Shulman, & Aloimonos, 2001).

Second, there are three models for computing optical flow in the literature. Besides gradient-based models there are frequency domain and correlation models, but computationally they are not very different. In all the models there is a stage in which smoothness assumptions are made and measurements within a region are combined. At this stage noisy estimates lead to bias (Fermüller et al., 2001).

There is a large number of motion experiments that also can be explained by our model.

A significant body of work on the integration of local velocity signals has been conducted in the context of moving plaids. Plaids are combinations of two wave gratings of different orientation, each moving with a constant speed. For any such "moving plaid" there is always some planar velocity the whole pattern can undergo which would produce exactly the same retinal stimulus. Depending on the parameters of the component gratings, the perception is of one coherent motion of the plaid or of two different motions of the gratings.

The motion of a coherent pattern can be found theoretically with the intersection of constraint model (IOC)—the vector component obtained from each individual grating constrains the local velocity vector to lie upon a line in velocity space, the intersection of the lines defines the motion of the plaid (Adelson & Movshon, 1982). However, often the perceived motion is different from the veridical. The error is influenced by

factors including orientation of the gratings, frequency, and contrast.

Ferrera and Wilson (1987) made a distinction between two kinds of plaids; in type I plaids the common motion is between the components motions of the two gratings, and in type II plaids the common motion lies outside the component directions. In case of equal contrast and frequency, for type II plaids the velocity is perceived towards the average of the component vectors (the VA) (Burke & Wenderoth, 1993; Ferrera & Wilson, 1990, 1991), whereas for type I plaids the estimate is largely veridical. For type I plaids if the contrast of the gratings is different the perceived velocity is closer in direction to the component of the grating of higher contrast (Kooi, Valois, Grosof, & Valois, 1992; Stoner, Albright, & Ramachandran, 1990). If the spatial frequency of the gratings differs (Smith & Edgar, 1991), the perceived motion is closer in direction to the gradients of higher spatial frequency than the IOC velocity. In no case is there an overestimate of the plaid velocity when compared to the IOC prediction.

Recalling that the plaid velocity is biased in direction toward the eigenvector of the larger eigenvalue of M', we can predict the expected bias from changes in the plaid pattern. For components of equal contrast and frequency, the major eigenvector is in the direction of the vector average of the component motion vectors. In type II plaids this results in an estimated flow towards the VA direction. If the contrast of one grating increases, the major eigenvector moves towards the direction of motion of that grating explaining the findings of Stoner et al. (1990) and Kooi et al. (1992). Higher frequencies in a direction amount to more measurements in that direction. In the case of orthogonal gratings, as in Smith and Edgar (1991), this results in an estimated flow closer in direction to the motion of the higher frequency.

Mingolla, Todd, and Norman (1992) studied stimuli consisting of lines moving behind apertures. The lines had one of two different orientations. For a motion to the right, and lines at orientation of 15° and 45° from the vertical, that is when the normal flow components were in the first quadrant (upwards and right) the motion appeared upward biased. With the normal flow components in the second quadrant (downwards and right—the lines at −15° and −45° from the vertical) the motion appeared downward biased and for symmetric lines (+15° and −15°) the motion was perceived as horizontal. As in the case of type II plaids, this can be predicted from the bias in flow estimation which changes the direction of the estimated flow towards the vector average direction.

Circular figures rotating in the image plane may not give the perception of a rigid rotation (Musatti, 1929; Wallach, 1935). The effect is well known for the spiral which appears to contract or expand depending whether the rotation is clockwise or counterclockwise. For a rotation around the spiral's center the motion vectors are tangential to circles and the normal flow vectors are close to the radial direction. This situation creates large bias in the regional estimation of flow and thus an additional motion component in the radial direction as illustrated in Fig. 22. This illusion, among many others, has been explained by Hildreth (1983) by means of a model of smooth flow. The smoothness constraint also contributes to radial motion as it penalizes positional change in flow. As discussed above, a complete flow model also needs to consider variation in the flow. However, even with small amounts of noise, the contribution of the bias to the radial motion component will be larger than the contribution from smoothness.

Noise in the normal flow measurements has been discussed before as a possible cause for misperceived motion. In Nakayama and Silverman (1988a, 1988b) and Ferrera and Wilson (1991) Monte Carlo experiments were performed to determine the expected value and variance of velocity calculated with the IOC method. The experiments proceeded by creating one-dimensional motion components which were corrupted with error of Gaussian distribution, and then computing for pairs of local velocity measurements the motion vector with the IOC model. The distribution of estimates created with this method was not found to be significantly biased away from the IOC prediction (Ferrera & Wilson, 1991) for the case of plaids, but the variance of these estimates was found to be correlated with the accuracy of directional perception (Nakayama & Silverman, 1988a).

Nakayama and Silverman (1988a, 1988b) found that smooth curves, including sinusoids, Gaussians and sigmoids may be perceived to deform non-rigidly when
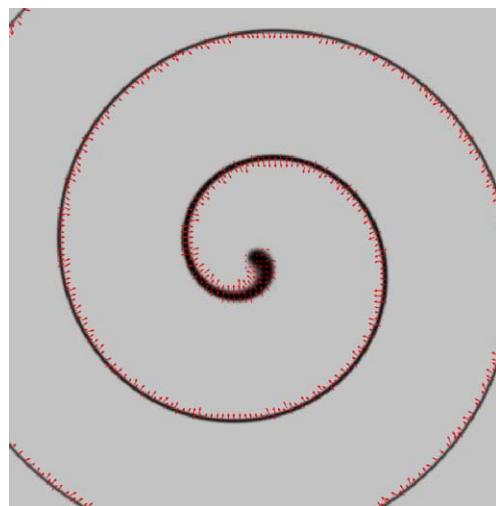

Fig. 22. A spiral rotating in the clockwise direction gives rise to a flow field with radially inward pointing vectors. The flow was derived using LS estimation within small circular regions. (No smoothness constraints were enforced.)
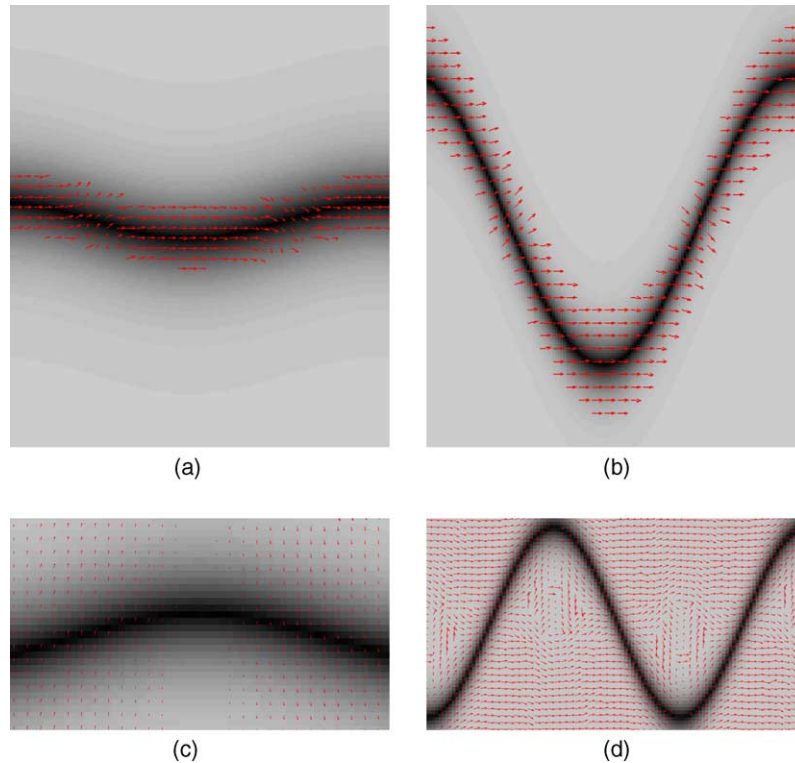
Fig. 23. (a, b) Regional LS estimation of flow. (c, d) Flow estimation using smoothness constraints.

translated in the image plane. For example, a sinusoid with low curvature (due to low amplitude or low frequency) moving with horizontal translation appears to deform non-rigidly, while the same motion for a sinusoid of high curvature appears veridical. In this case the main difference between the two curves lies in the amount of biased regional flow estimates as illustrated in Fig. 23. The flow field in Fig. 23a and b were estimated using LS estimation within small regions. As can be seen, in regions next to the inflexion point the flow vectors are biased upward on one side and downward on the other, and these regions are much smaller in the curve with larger curvature. The flow fields in Fig. 23c and d were estimated by enforcing in addition smoothness constraints. The smoothness propagates the bias, resulting in vertical flow components which are upward in half of the low curvature sinusoid and downward in the other half. In comparison the bias is much less in the high curvature sinusoid, effecting only the areas at the center of the curve.

Nakayama and Silverman (1988a) attributed the phenomenon to the large variance in the distribution of flow estimates. Clearly, the bias in regional flow estimates and the variance of the distribution of all the estimates are correlated; the larger the bias, the larger the variance. As Nakayama and Silverman (1988a) point out, the variance should be a good measure for the process of segmentation, that is to decide on coherence or non-coherence.

Simoncelli, Adelson, and Heeger (1991) and Weiss and Adelson (1998) also discuss noise in the normal flow estimates, but they only consider noise in the temporal derivatives. These noise terms do not cause bias; it is the noise in the spatial derivatives (i.e., the orientation of the local image velocity components) which causes bias. Weiss and Adelson, however, conclude bias in flow estimation using Bayesian modeling. Their explanation is based on the assumption that there is an a priori preference for small flow values. It is easily understood that this preference results in an increase in the a posteriori probabilty of small flow values and thus a bias towards underestimation of the flow, and thus a flow estimation similar to ours. Note, thus, in the Bayesian model the bias is in effect assumed, whereas in our model it is not. [1]

5. The theoretical question

The natural question to ask is whether the bias is due to the particular computations we described, or whether it is an inherent problem. In other words, is the estimation of features biased in whatever way it is conducted, or is bias a feature only of linear estimation? Are

---

[1] The non-Bayesian method of LS estimation implicitly also assumes priors; it assumes that all solutions have equal probability.

there other methods which do not suffer from bias to begin with, or is it maybe possible to estimate the bias and then correct for it? Our answer is, in general it is not. This section is a brief statistical discussion explaining what could be done, why it is very hard to correct for the bias and that the theoretically best thing to do is to partially correct for it.

The mathematical problem at hand (for edge intersection and flow estimation) is to find a solution to an over-determined system of equation of the form $A\vec{x} = \vec{b}$. The observations A and $\vec{b}$ are corrupted by noise, i.e., $A = A' + \delta A$ and $\vec{b} = \vec{b}' + \delta \vec{b}$. In addition there is system error, $\vec{\epsilon}$ (because the equations are only approximations), and thus $A'\vec{x} = \vec{b}' + \vec{\epsilon}$. We are dealing with, what is called in statistical regression the *errors in variable* (EIV) model.

It is well known, that the least squares (LS) estimator is biased (Fuller, 1987). The LS solution, which is linear in $\vec{b}$, is an asymptotically unbiased estimator only, when the errors δA are 0 and the errors $\delta \vec{b}$ are independent.

The classical way to address the problem is by means of the corrected least squares (CLS) estimator. If the statistics of the noise, that is the covariance matrix of δA, were known, an asymptotically unbiased linear estimation could be obtained. The problem is that for small amounts of data, accurate estimation of the variance of the noise is a very difficult problem. In this case, the estimation of the variance is not accurate, leading to large variance for CLS.

In recent years the technique of total least squares (TLS) has received a lot of attention. The basic idea underlying this non-linear technique is to deal with the errors in A and $\vec{b}$ symmetrically. If all the errors in δA and $\delta \vec{b}$ are identical and independent, TLS is asymptotically unbiased. In the case they are not, one would need to whiten the data. But this requires the estimation of the ratio of the error variances δA and $\delta \vec{b}$, which is at least as hard as obtaining the variance of δA. An incorrect value of the ratio often results in an unacceptably large *over correction* for the bias. However, the main problem for TLS is system error. Theoretically one can use multiple tests to obtain the measurement errors, like re-measuring or re-sampling; but unless the exact parameters of the model are known, one cannot test for system error.

Re-sampling techniques, such as bootstrap and Jackknife have been discussed for bias correction. These techniques can correct for the error term which is inverse proportional to the number of data points (i.e., $O(1/n)$), and thus they can improve the estimate of the mean for unbiased estimators. However, these techniques cannot correct for the bias (Efron & Tibshirani, 1993). They are useful for estimating the variance in order to provide confidence intervals.

Why is it so difficult to obtain accurate estimates of the noise parameters? To acquire a good noise statistic a lot of data is required, so data needs to be taken from large spatial areas acquired over a period of time, but the models used for the estimation can only be assumed to hold locally. Thus to integrate more data, models of the scene need to be acquired. Specifically, in the case of intersecting lines, first long edges and bars need to be detected, and in the case of motion, first discontinuities due to changes in depth and differently moving entities need to be detected and the scene segmented. If the noise parameters stayed fixed for extended periods of time it would be possible to acquire enough data to closely approximate these parameters, but usually the noise parameters do not stay fixed long enough. Sensor characteristics may stay fixed, but there are many other sources of noise besides sensor noise. The lighting conditions, the physical properties of the objects being viewed, the orientation of the viewer in 3D space, and the sequence of eye movements all have influences on the noise.

Clearly, bias is not the only thing that matters. There is a trade-off between bias and variance. Generally, an estimator correcting for bias increases the variance while decreasing the bias. Very often, the mean squared error (MSE) is used as a criterion for the performance of an estimator. It is the expected value of the square of the difference between the estimated and the true value. If x' is used to denote the actual value, $\hat{x}$ to denote the estimate, and $E(\cdot)$ to denote the expected values, the MSE is defined as

$$\mathrm{MSE}(\hat{x}) = E((\hat{x} - x')^2) = (E(\hat{x}) - x')^2 + E(x' - E(\hat{x}))^2$$
$$= \mathrm{bias}^2(\hat{x}) + \mathrm{cov}(\hat{x}) \tag{11}$$

that is, as the sum of the square of the bias (denoted as $\mathrm{bias}(\hat{x})$) and the variance (denoted as $\mathrm{cov}(\hat{x})$). Based on the criterion of minimizing the MSE, there are compromised estimators which outperform both uncorrected biased estimators and corrected unbiased estimators. The ideal linear estimator would perform a partial bias correction using CLS. In Appendix B we derive how much this correction (theoretically) should be. It depends on the covariance of the LS estimates. The larger the covariance, the less correction.

This brings us to the point of a psychometric function describing quantitatively the effects of noise on the perception. We should assume that our vision system is doing its best and thus has learned to correct whenever it has data available to obtain estimates of the noise. Since the correction should depend on the variance, a measure of misestimation should involve both the bias and the variance of the LS estimator; we suggest to investigate a weighted sum of these two components. Such a measure may explain why the illusory perception in some of the patterns weakens after extended viewing, in particular when subjects are asked to fixate (Helmholtz, 1962; Yo & Wilson, 1992). In this case, we can assume the noise

parameters stay fixed, and the visual system can reasonably well estimate them. Furthermore, such a measure would predict that the density of a pattern should have an influence on the perception, with slightly more accurate estimates for denser patterns.

Finally, one may think there are ways to correct the bias without using statistics. The bias depends on the gradient distribution, that is the directions of edgels or motion measurements. Since an uneven distribution (corresponding to an ill-conditioned matrix M) leads to a large bias, one may want to normalize for direction. We could do so, if we had very large amounts of data. However, with few measurements we cannot. Consider that there are only two directions. It would mean that we give more weight to the direction with few measurements, which has large variance, and lesser weight to the other direction which has smaller variance. With few measurements only, this could lead to large over correction.

Also, it should be clear that in our models of feature estimation, we cannot employ higher-level knowledge about the structure of the scene. For example, computing the intersection of lines by first estimating the average direction of each individual line and then intersecting the lines, would not give bias. But, this would require that the noisy elements are classified first into two categories. The same applies for the flow in plaids. If we wanted to estimate the motion of the individual gratings, we would first need to understand that there are exactly two different directions and classify the motion components. If, as in Ferrera and Wilson (1991) pairs of noisy measurements are intersected, and the elements are randomly sampled (without classifying them first) there will be a bias in the direction of the flow component with more measurements. If the elements are segmented and each pair has an element of either grating, there should be a slight overestimation in magnitude. This is, because the underestimation in LS results from the asymptotic behavior; terms linear in $1/n$ or higher do not effect the bias, but these terms for very few measurements, i.e., two in this case, cause a bias in the opposite direction.

6. Discussion

6.1. Theories of illusions

Theories about illusions have been formulated ever since their discovery. Many of the theories are aimed only at one specific illusion and most of the early theories would be seen nowadays as adding little to a mere description of the illusion. Most theories which attempt to explain a broad spectrum of illusions are based on a specific sort of mechanism which has been suggested to explain the workings of human visual perception. These mechanisms are either hypothetical, based on physical analogies, or general observations about the physiology and architecture of the brain (for example, lateral inhibition). The theory proposed here is of a mathematical nature based on the geometry and statistics of capturing light rays and computing their properties (gray values and spatio-temporal derivatives), and thus it applies to any vision system, artificial or biological. However, one might find that our theory resembles some existing theories if they are put in a statistical framework.

Chiang (1968) proposed a retinal theory that applies to patterns in which lines running close together affect one another. He likened the light coming into the eye from two lines to the light falling onto a screen from two slit sources in the study of diffraction patterns. This is because of the blurring and diffusing effect of the medium and the construction of the eye. The perceived locations of the lines are at the peaks of their distributions; thus two close lines influence each other's locations and become one when the sum of their distributions forms a single peak. This leads to an overestimation of acute angles, and provides an explanation of the Zöllner, Poggendorff, and related illusions as well as the Müller-Lyer effect. Glass (1970) discussed optical blurring as a cause for the perceptual enlargement of acute angles as it fills in the angle at line intersections and he proposed this as an explanation of the Zöllner and Poggendorff effect. Ginsburg argued that neural blurring occurs because of lateral inhibition and this has the effect of spatial frequency filtering. In Ginsburg (1975) he suggested that low frequency attenuation contributes to the formation of the illusory Kanizsa triangle and in Ginsburg (1984) he discussed filtering processes as a cause for the Müller-Lyer illusion. In a number of recent studies band-pass filtering has been proposed as a cause of geometrical optical illusions; Morgan and Moulden (1986), and Earle and Maskell (1993) discuss linear band-pass filters as a cause of the café wall illusion. Morgan and Casco (1990) discuss band-pass filtering in conjunction with second-order stage filters that extract features in the Zöllner and Judd illusion. Bulatov et al. (1997) propose an elaborate neurophysiological model and they discuss the Müller-Lyer and Oppel–Kundt illusion. Morgan (1999) suggests blurring in second stage filters as the main cause of the Poggendorff illusion and (Morgan & Glennerster, 1991; Morgan, Hole, & Glennerster, 1990) discuss large receptive second stage eclectic units, which obtain as input heterogeneous features from smaller subfields, as cause for the Müller-Lyer illusion.

The diffraction in Chiang's model, the optical and neural blurring in later models, amounts to uncertainty in the location of the perceived gray-level values, or they can be interpreted as noise occurring somewhere in the image formation or the image processing. Thus the concept of uncertainty is invoked in vague ways in these

studies. The models that have been discussed are, how-ever, very restricted. They apply to particular processes, either on the retina or the neural hardware.

There are a number of theories in which eye move-ments are advanced as an important causative factor in illusions. Our theory also proposes that eye movements play a role because they are a relevant source of noise. The particular eye movements made in looking at a pattern influence the noise distribution and thus the bias perceived, but there are other noise sources besides eye movements, and this predicts the existence of illusory effects for some patterns even under fixation or tachis-toscopic viewing.

Helmholtz (1962) suggested that ocular movements are of importance in some illusions, but he also ex-pressed doubt that they could be the main source, as other illusions are not influenced by them. Carr (1935) proposed that the eyes react to accessory lines and as a result pass more easily over unfilled than filled elements. In the Müller-Lyer figures the eyes move more freely over the figure with outgoing fins than over the one with ingoing fins, and in the Poggendorff and Zöllner figures deflections and hesitations in the eye movements are associated with the intersections of the long lines with the obliques. Piaget (1961) proposed a "law of relative centrations." By "centration" he refers to a kind of centering of attention which is very much related to fixation. Centration on part of the field causes an overestimation of that part relative to the rest of the field. Virsu (1971) suggested that a tendency to eye movements, that is, instructions for eye movements, has a perceptual effect. He suggests that the eye movements most readily made are linear and rectilinear, horizontal or vertical. When viewing lines which lie off the vertical or horizontal, an eye movement correction must take place and this can give rise to perceptual distortion.

Other theories include those whose main objective was the explanation of figural aftereffects applied to illusions (Ganz, 1966; Köhler & Wallach, 1944). In these theories interference between nearby lines occurs be-cause of satiation in the cortex or lateral inhibition processes. There are also theories based on the assumption that the perceptual system interprets illusory patterns as flat projections of three-dimensional displays (Tausch, 1954; Thiéry, 1896). The most detailed and most popular such theory is due to Gregory (1963), who invokes "size constancy scaling," which can be triggered in two different ways, either unconsciously or by higher-level awareness.

6.2. Illusions of size

Following Boring (1942), patterns which are called geometrical optical illusions may be classified roughly into two categories: illusions of direction (where orien-tation of a line or figure is misjudged) and illusions of extent (where size or length is misjudged). The patterns discussed so far are in the first class. They have been explained on the basis of noise in the local measure-ments. Most illusions in the second class could be ex-plained if noise were present in the representations of quantities which cover larger regions. Such noise may be attributed to the processing in the visual system. From evidence we have about the varying size of receptive fields, it is understood that images are processed at multiple levels of resolution (Zeki, 1993). Since the higher-level processes of segmentation and recognition need information from large parts of the image, there must be processes that combine information from local neighborhoods into representations of global informa-tion, and these processes may carry uncertainty.

Intuitively, noise effecting regions of larger spatial extent, causes blurring over these regions. Thus, neigh-boring parts in a figure influence each other and as a result they are perceived closer in distance. This obser-vation can explain most of the significant illusions in the second class which are: the contrast effect; the illusion of filled and unfilled extent, that is, the effect that a filled extent is overestimated when compared with an unfilled extent (an example is the Oppel–Kundt illusion (Kundt, 1863)); the framing effect, that is, the overestimation of framed objects; and the flattening of arcs, that is, the effect that short arcs are perceptually flattened. Take as an example the Delboeuf illusion (Delboeuf, 1892)—two concentric circles with the outer one perceptually de-creased and the inner one increased. Blurring which ef-fects both circles will cause the inner one to expand and the outer one to contract. Another example is the fa-mous Müller-Lyer illusion. Bias in the intersection points due to noise in local measurements can account for a small size change in the vertical lines, but it re-quires noise in larger regions to account for significant size changes as experienced with this pattern. Similarly, such noise will increase the effect in the Poggendorff illusion, and it may account for the perception in vari-ations of this pattern.

6.3. Bias in 3D

Many other computations in the visual system, be-sides feature extraction, are estimation processes. Clearly, the visual recovery processes are estimations—that is, the computations which extract physical and geometrical properties of the scene by inverting the (optical and geometrical) image formation. Examples are the estimations of the light source, the motion, the structure and shape of the scene and the material properties of surfaces.

We recently started investigating these computations. Results are available for shape from motion, stereo and texture from all three known cues, that is foreshorten-ing, scaling and position (Hui & Fermüller, 2003). We

analyzed the bias and found that it is consistent with what is empirically known about the estimation of shape. It has been observed from computational as well as psychophysical experiments, that for many configurations there is a tendency to underestimate the slant. (The slant refers to the angle between the surface normal and the optical axis.) In other words, the scene appears compressed in the depth dimension. The bias predicts this underestimation of slant.

We created an illusory display demonstrating the effect for 3D motion which can be viewed at (Fermüller, 2003). It shows a plane with two textures, one in the upper half, one in the lower half. The camera moves around the plane while fixating on its center. Because the bias in the upper texture is much larger than in the lower one, the plane appears to be segmented into two parts, with the upper part of much smaller slant. This should demonstrate our point. The bias not only is a problem of 2D vision, but of 3D vision as well.

Appendix A. Expected value of the least squares solution

In this section a second-order Taylor expansion of the expected values of the least squares solution for both the intersection point (Section 3) and the flow (Section 4) is given.

Let $\vec{y}$ be the vector to be estimated, that is, either the intersection point $\vec{x}$ or the flow $\vec{u}$. I_s is the matrix consisting of the spatial derivatives I_{x_i}, I_{y_i}. $\vec{c}$ in Section 3 is the vector of temporal derivatives I_{t_i} and $\vec{c}$ in Section 4 is the vector whose elements are $I_{x_i} x_{0_i} + I_{y_i} y_{0_i}$.

The expected value $E(\vec{y})$ of the least squares solution is given by

$$E(\vec{y}) = E\left((I_s^T I_s)^{-1} (I_s^T \vec{c}) \right)$$

As the noise is assumed to be independent and zero-mean, the first-order terms as well as the second-order terms in the noise of the temporal derivatives (or the positional parameters) vanish. This means that it is only the noise in the spatial derivatives which causes bias in the mean. The expansion at points $N = 0$ (i.e., $\delta I_{x_i} = \delta I_{y_i} = \delta I_{t_i} = 0$ or $\delta I_{x_i} = \delta I_{y_i} = \delta x_{0_i} = \delta y_{0_i} = 0$) can be written as

$$E(\vec{y}) = \vec{y}' + \sum_i \left(\left. \frac{\partial^2 \vec{y}}{\partial \delta I_{x_i}^2} \right|_{N=0} \frac{E(\delta I_{x_i}^2)}{2} + \left. \frac{\partial^2 \vec{y}}{\partial \delta I_{y_i}^2} \right|_{N=0} \frac{E(\delta I_{y_i}^2)}{2} \right)$$

For notational simplicity, we define

$$M = I_s^T I_s, \quad \vec{b} = I_s^T \vec{c}$$
$$M' = I_s'^T I_s', \quad \vec{b}' = I_s'^T \vec{c}'$$

To compute the partial derivatives, the explicit terms of the matrix M are

$$M = \begin{bmatrix} \sum_i (I'_{x_i} + \delta I_{x_i})^2 & \sum_i (I'_{x_i} + \delta I_{x_i})(I'_{y_i} + \delta I_{y_i}) \\ \sum_i (I'_{x_i} + \delta I_{x_i})(I'_{y_i} + \delta I_{y_i}) & \sum_i (I'_{y_i} + \delta I_{y_i})^2 \end{bmatrix}$$

and the terms of $\vec{b}$ are

$$\vec{b} = \begin{bmatrix} \sum_i (I'_{x_i} + \delta I_{x_i})(I'_{t_i} + \delta I_{t_i}) \\ \sum_i (I'_{y_i} + \delta I_{y_i})(I'_{t_i} + \delta I_{t_i}) \end{bmatrix}$$

and

$$\vec{b} = \begin{bmatrix} \sum_i (I'_{x_i} + \delta I_{x_i})^2 (x'_{0_i} + \delta x_{0_i}) \\ +(I'_{x_i} + \delta I_{x_i})(I'_{y_i} + \delta I_{y_i})(y'_{0_i} + \delta y_{0_i}) \\ \sum_i (I'_{x_i} + \delta I_{x_i})(I'_{y_i} + \delta I_{y_i})(x'_{0_i} + \delta x_{0_i}) \\ +(I'_{y_i} + \delta I_{y_i})^2 (y'_{0_i} + \delta y_{0_i}) \end{bmatrix}$$

Using the fact that for an arbitrary matrix Q

$$\frac{-\partial Q^{-1}}{\partial x} = Q^{-1} \frac{\partial Q}{\partial x} Q^{-1}$$

we find the first-order and second-order derivatives to be

$$\frac{\partial \vec{y}}{\partial \delta I_{x_i}} = -M^{-1} \begin{bmatrix} 2I_{x_i} & I_{y_i} \\ I_{y_i} & 0 \end{bmatrix} M^{-1} \vec{b} + M^{-1} \frac{\partial \vec{b}}{\partial \delta I_{x_i}}$$

$$\frac{\partial^2 \vec{y}}{\partial \delta I_{x_i}^2} = 2M^{-1} \begin{bmatrix} 2I_{x_i} & I_{y_i} \\ I_{y_i} & 0 \end{bmatrix} M^{-1} \begin{bmatrix} 2I_{x_i} & I_{y_i} \\ I_{y_i} & 0 \end{bmatrix} M^{-1} \vec{b}$$
$$- M^{-1} \begin{bmatrix} 2 & 0 \\ 0 & 0 \end{bmatrix} M^{-1} \vec{b} - 2M^{-1} \begin{bmatrix} 2I_{x_i} & I_{y_i} \\ I_{y_i} & 0 \end{bmatrix} M^{-1} \frac{\partial \vec{b}}{\partial \delta I_{x_i}}$$
$$+ M^{-1} \frac{\partial^2 \vec{b}}{\partial \delta I_{x_i}^2}$$

and similarly we have symmetric expressions for

$$\frac{\partial \vec{y}}{\partial \delta I_{y_i}} \quad \text{and} \quad \frac{\partial^2 \vec{y}}{\partial \delta I_{y_i}^2}$$

Since we assume $E(\delta I_{x_i}^2) = E(\delta I_{y_i}^2) = \sigma_s^2$, the expansion can thus be simplified to

$$E(\vec{y}) = \vec{y}' - \underline{nM'^{-1} \vec{y}' \sigma_s^2} + \underline{\sum_{i=1}^n M'^{-1} \left(\frac{\partial^2 \vec{b}}{\partial \delta I_{x_i}^2} + \frac{\partial^2 \vec{b}}{\partial \delta I_{y_i}^2} \right) \Big|_{N=0} \frac{\sigma_s^2}{2}}$$
$$+ \sum_i \left\{ M'^{-1} \left(\begin{bmatrix} 2I'_{x_i} & I'_{y_i} \\ I'_{y_i} & 0 \end{bmatrix} M'^{-1} \begin{bmatrix} 2I'_{x_i} & I'_{y_i} \\ I'_{y_i} & 0 \end{bmatrix} \right. \right.$$
$$+ \begin{bmatrix} 0 & I'_{x_i} \\ I'_{x_i} & 2I'_{y_i} \end{bmatrix} M'^{-1} \begin{bmatrix} 0 & I'_{x_i} \\ I_{x_i} & 2I'_{y_i} \end{bmatrix} \right) \vec{y}'$$
$$- M'^{-1} \left(\begin{bmatrix} 2I'_{x_i} & I'_{y_i} \\ I'_{y_i} & 0 \end{bmatrix} M'^{-1} \frac{\partial \vec{b}}{\partial \delta I_{x_i}} \Big|_{N=0} \right.$$
$$\left. \left. + \begin{bmatrix} 0 & I'_{x_i} \\ I'_{x_i} & 2I'_{y_i} \end{bmatrix} M'^{-1} \frac{\partial \vec{b}}{\partial \delta I_{y_i}} \Big|_{N=0} \right) \right\} \sigma_s^2$$

where we have underlined the terms that do not depend on n (where n is the number of measurements being combined in a region). These terms will give a consis-

tent, statistically constant response. The rest of the terms diminish proportionally to $1/n$. Informal experiments show that these terms become negligible for $n > 5$, a number clearly smaller than the number of terms likely to be combined in any real system.

In the analysis of Section 3, the elements of $\vec{c}$ are $I_{x_i} x_{0_i} + I_{y_i} y_{0_i}$; thus

$$\frac{\partial \vec{b}}{\partial \delta I_{x_i}}\bigg|_{N=0} = \begin{bmatrix} 2I'_{x_i} x'_{0_i} + I'_{y_i} y'_{0_i} \\ I'_{y_i} x'_{0_i} \end{bmatrix} \quad \frac{\partial^2 \vec{b}}{\partial \delta I_{x_i}^2}\bigg|_{N=0} = \begin{bmatrix} 2x'_{0_i} \\ 0 \end{bmatrix}$$

$$\frac{\partial \vec{b}}{\partial \delta I_{y_i}}\bigg|_{N=0} = \begin{bmatrix} I'_{x_i} y'_{0_i} \\ I'_{x_i} x'_{0_i} + 2I'_{y_i} y'_{0_i} \end{bmatrix} \quad \frac{\partial^2 \vec{b}}{\partial \delta I_{y_i}^2}\bigg|_{N=0} = \begin{bmatrix} 0 \\ 2y'_{0_i} \end{bmatrix}$$

and the main terms in the expected value of the intersection point $E(\vec{x})$ are

$$E(\vec{x}) = \vec{x}' - nM'^{-1} \vec{x}' \sigma_s^2 + M'^{-1} \begin{bmatrix} \sum x'_{0_i} \\ \sum y'_{0_i} \end{bmatrix} \sigma_s^2$$

or

$$E(\vec{x}) = \vec{x}' + nM'^{-1} (\vec{\bar{x}}'_0 - \vec{x}') \sigma_s^2$$

where $\vec{\bar{x}}'_0$ denotes the mean of the values $\vec{x}'_{0_i}$.

In the analysis in Section 4 the elements of $\vec{c}$ are I_{t_i}. Thus the first-order derivatives are

$$\frac{\partial \vec{b}}{\partial \delta I_{x_i}}\bigg|_{N=0} = \begin{bmatrix} I'_{t_i} \\ 0 \end{bmatrix} \quad \text{and} \quad \frac{\partial \vec{b}}{\partial \delta I_{y_i}}\bigg|_{N=0} = \begin{bmatrix} 0 \\ I'_{t_i} \end{bmatrix}$$

and the second-order derivatives vanish. The expected value of the flow $E(\vec{u})$ simplifies to

$$E(\vec{u}) = \vec{u}' - nM'^{-1} \vec{u}' \sigma_s^2.$$

Appendix B. Bias correction

Let us write the equation system as $A\vec{x} = \vec{b}$. Let $\vec{x}_{LS}$ denote the LS estimator for the errors in variable model. It's expected bias amounts to

$$\text{bias}(\vec{x}_{LS}) = \lim_{n \to \infty} E(\vec{x}_{LS} - \vec{x}') = -\sigma^2 \left(\lim_{n \to \infty} \left(\frac{1}{n} A^{\mathrm{T}} A' \right) \right)^{-1} \vec{x}'$$

Assuming the variance of the error δA is known, the bias can be removed with the CLS estimator, which amounts to

$$\vec{x}_{CLS} = (A^{\mathrm{T}} A - n\sigma^2 I)^{-1} (A^{\mathrm{T}} \vec{b})$$

and can be rewritten as

$$\vec{x}_{CLS} = (I - n\sigma^2 (A^{\mathrm{T}} A)^{-1})^{-1} \vec{x}_{LS}$$

Denoting the variance as $\text{cov}(\cdot)$, the variance of $\vec{x}_{CLS}$ amounts to

$$\text{cov}(\vec{x}_{CLS}) = (I - n\sigma^2 (A^{\mathrm{T}} A)^{-1})^{-2} \text{cov}(\vec{x}_{LS})$$

Let us now investigate what the theoretically best linear estimator should be. We have to adjust the corrected least squares estimator, such that we achieve smaller MSE (as defined in Eq. (11)). Let $x_\alpha = \alpha \vec{x}_{CLS} + (1 - \alpha) \vec{x}_{LS}$ denote the adjusted CLS estimator.

Then we have that

$$\text{MSE}(x_\alpha) = \alpha^2 \text{cov}(\vec{x}_{CLS}) + (1 - \alpha)^2 \text{bias}^2(\vec{x}_{LS})$$
$$= \alpha^2 (I - n\sigma^2 (A^{\mathrm{T}} A)^{-1})^{-2} \text{cov}(\vec{x}_{LS})$$
$$+ (1 - \alpha)^2 \text{bias}^2(\vec{x}_{LS})$$

which is a quadratic expression. Thus, the MSE minimum is achieved for

$$\alpha = \frac{\text{bias}^2(\vec{x}_{LS})}{\text{bias}^2(\vec{x}_{LS}) + \text{cov}(\vec{x}_{LS})(I - n\sigma^2 (A^{\mathrm{T}} A)^{-1})^{-2}}$$

This shows that according to the MSE criterion a less bias corrected x_α is better than a bias corrected $\vec{x}_{CLS}$. The larger the variance of the LS estimates, the less the correction should be.

References

Adelson, E. H., & Movshon, J. A. (1982). Phenomenal coherence of moving visual patterns. *Nature, 300*(December), 523–525.

Blasdel, G. G. (1992). Differential imaging of ocular dominance and orientation selectivity in monkey striate cortex. *Journal of Neuroscience, 12*, 3115–3138.

Boring, E. G. (1942). *Sensation and perception in the history of experimental psychology*. New York: Appleton-Century-Crofts.

Bulatov, A., Bertulis, A., & Mickiene, L. (1997). Geometrical illusions: Study and modelling. *Biological Cybernetics, 77*, 395–406.

Burke, D., & Wenderoth, P. (1993). The effect of interactions between one-dimensional component gratings on two-dimensional motion perception. *Vision Research, 33*, 343–350.

Cameron, E., & Steele, W. (1905). The Poggendorff illusion. *Psychological Monographs, 7*, 83–107.

Canny, J. (1986). A computational approach to edge detection. *IEEE Transactions on Pattern Analysis and Machine Intelligence, 8*, 679–698.

Carpenter, R. H. S. (1988). *Movements of the eye*. London: Pion.

Carr, H. A. (1935). *An introduction to space perception*. Green, New York: Longmans.

Chiang, C. (1968). A new theory to explain geometrical illusions produced by crossing lines. *Perception and Psychophysics, 3*, 174–176.

Delboeuf, J. L. R. (1892). Sur une nouvelle illusion d'optique. *Bulletin de l'Academie Royale de Belgique, 24*, 545–558.

Earle, D. C., & Maskell, S. (1993). Fraser cords and reversal of the café wall illusion. *Perception, 22*, 383–390.

Efron, B., & Tibshirani, R. (1993). *An introduction to the boostrap*. Chapman & Hall.

Fermüller, C. (2003). Available: http://www.optical-illusions.org.

Fermüller, C., Pless, R., & Aloimonos, Y. (2000). The Ouchi illusion as an artifact of biased flow estimation. *Vision Research, 40*, 77–96.

Fermüller, C., Shulman, D., & Aloimonos, Y. (2001). The statistics of optical flow. *Computer Vision and Image Understanding, 82*, 1–32.

Ferrera, V. P., & Wilson, H. R. (1987). Direction specific masking and the analysis of motion in two dimensions. *Vision Research, 27*, 1783–1796.

Ferrera, V. P., & Wilson, H. R. (1990). Perceived direction of two-dimensional moving patterns. *Vision Research, 30*, 273–287.

Ferrera, V. P., & Wilson, H. R. (1991). Perceived speed of moving two-dimensional patterns. *Vision Research, 31*, 877–893.

Fraser, J. (1908). A new visual illusion of direction. *British Journal of Psychology, 2*, 307–320.

Fuller, W. (1987). *Measurement error models*. New York: Wiley.

Furmanski, C., & Engel, S. (2000). An oblique effect in human primary visual cortex. *Nature Neuroscience, 3*, 535–536.

Ganz, L. (1966). Mechanism of the F.A.E.'s. *Psychological Review, 73*, 128–150.

Gillam, B. (1998). Illusions at century's end. In *Perception and cognition at century's end* (pp. 95–136). Academic Press.

Ginsburg, A. P. (1975). Is the illusory triangle physical or imaginary? *Nature, 257*, 219–220.

Ginsburg, A. P. (1984). Visual form perception based on biological filtering. In L. Spillman & B. R. Wooton (Eds.), *Sensory experience, adaptation and perception* (pp. 53–72). New Jersey: L. Erlbaum.

Glass, L. (1970). Effect of blurring on perception of a simple geometric pattern. *Nature, 228*, 1341–1342.

Green, R., & Hoyle, G. (1964). Adaptation level and the optic-geometric illusions. *Nature, 201*, 1200–1201.

Gregory, R. L. (1963). Distortion of visual space as inappropriate constancy scaling. *Nature, 119*, 678–680.

Grossberg, S., & Mingolla, E. (1985a). Neural dynamics of form perception: Boundary completion, illusory figures, and neon color spreading. *Psychological Review, 92*(2), 173–211.

Grossberg, S., & Mingolla, E. (1985b). Neural dynamics of perceptual grouping: Textures, boundaries and emergent segmentations. *Perception and Psychophysics, 38*(2), 141–171.

Helmholtz, H. L. F. V. (1962). *Treatise on physiological optics* (Vol. III). New York: Dover, translated from the third German edition by J.P.C. Southall.

Hering, E. (1861). *Beiträge zur Psychologie* (Vol. 1). Leipzig: Engelman.

Hildreth, E. (1983). *The measurement of visual motion*. Cambridge, MA: MIT Press.

Horn, B. K. P. (1986). *Robot vision*. New York: McGraw-Hill.

Horn, B. K. P., & Schunk, B. G. (1981). Determining optical flow. *Artificial Intelligence, 17*, 185–203.

Howard, I., & Templeton, W. (1966). *Human spatial orientation*. New York: Wiley.

Hubel, D., & Wiesel, T. (1968). Receptive fields and functional architecture of the monkey striate cortex. *Journal of Physiology (London), 195*, 215–243.

Hubel, D. H., & Wiesel, T. N. (1961). Integrative action in the cat's lateral geniculate body. *Journal of Physiology (London), 155*, 385–398.

Hui, J., & Fermüller, C. (2003). Uncertainty in 3d shape estimation. In *Proceedings of the 3rd international workshop on statistical and computational theories of vision*, to appear.

Judd, C., & Courten, H. (1905). The Zöllner illusion. *Psychological Monographs, 7*, 112–139.

Kitaoka, A. (2003). Available: http://www.ritsumei.ac.jp/akitaoka/index-e.html.

Koenderink, J. J. (1984). The structure of images. *Biological Cybernetics, 50*, 363–370.

Köhler, W., & Wallach, H. (1944). Figural after-effects: An investigation of visual processes. *Proceedings of the American Philosophical Society, 88*, 269–357.

Kooi, F. L., Valois, K. K. D., Grosof, D. H., & Valois, R. L. D. (1992). Properties of the recombination of one-dimensional motion signals into a pattern motion signal. *Perception and Psychophysics, 52*, 415–424.

Kundt, A. (1863). Annalen der Physik und Chemie. Untersuchungen über Augenmaß und optische Täuschungen. *Pogg. Ann., 120*, 118–158.

Leibowitz, H., & Toffey, S. (1966). The effects of rotation and tilt on the magnitude of the Poggendorff illusion. *Vision Research, 6*, 101–103.

Lindeberg, T. (1994). *Scale-space theory in computer vision*. Boston: Kluwer.

Lukiesh, M. (1922). *Visual illusions*. New York: Dover.

Marr, D., & Hildreth, E. C. (1980). A theory of edge detection. *Proceedings of the Royal Society of London B, 207*, 187–217.

Mingolla, J., Todd, J., & Norman, J. (1992). The perception of globally coherent motion. *Vision Research, 32*, 1015–1031.

Morgan, M. J. (1999). The Poggendorff illusion: A bias in the estimation of the orientation of virtual lines by second-stage filters. *Vision Research, 39*, 2361–2380.

Morgan, M. J., & Casco, C. (1990). Spatial filtering and spatial primitives in early vision: An explanation of the Zöllner–Judd class of geometrical illusions. *Proceedings of the Royal Society of London B, 242*, 1–10.

Morgan, M. J., & Glennerster, A. (1991). Efficiency of locating centres of dot clusters by human observers. *Vision Research, 31*, 2075–2083.

Morgan, M. J., Hole, G., & Glennerster, A. (1990). Biases and sensitivities in the geometrical illusions. *Vision Research, 30*, 1793–1810.

Morgan, M. J., & Hoptopf, N. (1989). Perceived diagonals in grids and lattices. *Vision Research, 29*, 1005–1015.

Morgan, M. J., & Moulden, B. (1986). The Münsterberg figure and twisted cords. *Vision Research, 26*(11), 1793–1800.

Morinaga, S. (1933). Untersuchungen über die Zöllnersche Täuschung. *Japanese Journal of Psychology, 8*, 195–242.

Müller-Lyer, F. C. (1896). Zur Lehre von den optischen Täuschungen: Über Kontrast und Konfluxion. *Zeitschrift Fur Psychologie, 9*, 1–16.

Musatti, C. (1929). Sui fenomeni stereocinetici. *Archivio Italiano di Psicologia, 3*, 105–120.

Nakayama, K., & Silverman, G. H. (1988a). The aperture problem—I: Perception of nonrigidity and motion direction in translating sinusoidal lines. *Vision Research, 28*, 739–746.

Nakayama, K., & Silverman, G. H. (1988b). The aperture problem—II: Spatial integration of velocity information along contours. *Vision Research, 28*, 747–753.

Oppel, J. J. (1855). *Über geometrisch-optische Täuschungen* (pp. 37–47). Jahresbericht Phys. Ver. Frankfurt.

Orbison, W. (1939). Shape as a function of the vector field. *American Journal of Psychology, 52*, 31–45.

Ouchi, H. (1977). *Japanese and geometrical art*. New York: Dover.

Oyama, T. (1960). Japanese studies on the so-called geometrical–optical illusions. *Psychologia, 3*, 7–20.

Palmer, S. E. (1999). *Vision science: photons to phenomenology*. Cambridge, MA: MIT Press.

Piaget, J. (1961). *Les Mechanismes Perceptifs*. Presses Universitaires de Gravee, translated by G.N. Seagrim as The Mechanisms of Perception, Routledge & Kegan Paul, London, 1969.

Pinna, B., & Brelstaff, G. J. (2000). A new visual illusion of relative motion. *Vision Research, 40*(16), 2091–2096.

Robinson, J. O. (1972). *The psychology of visual illusion*. London: Hutchinson.

Simoncelli, E. P., Adelson, E. H., & Heeger, D. J. (1991). Probability distributions of optical flow. In *Proceedings of the IEEE conference on computer vision and pattern recognition, Maui, Hawaii* (pp. 310–315).

Smith, A. T., & Edgar, G. K. (1991). Perceived speed and direction of complex gratings and plaids. *Journal of the Optical Society of America, 8*, 1161–1171.

Stoner, G. R., Albright, T. D., & Ramachandran, V. S. (1990). Transparency and coherence in human motion perception. *Nature, 344*, 153–155.

Tausch, R. (1954). Optische Täuschungen als artifizielle Effekte der Gestaltungsprozesse von Größen und Formkonstanz in der natürlichen Raumwahrnehmung. *Psychologische Forschung, 24*, 299–348.

Thiéry, A. (1896). Über geometrisch optische Täuschungen. *Philosophical Studies, 12*, 67–126.

Virsu, V. (1971). Tendencies to eye movement, and misperception of curvature, direction and length. *Perception and Psychophysics, 9*, 65–72.

Wagner, H. (1969). *Simultaneous and successive contour displacements*. Ph.D. thesis, University of Wales.

Wallace, G. (1969). The critical distance of interaction in the Zöllner illusion. *Perception and Psychophysics, 5*, 261–264.

Wallace, G., & Crampin, D. (1969). The effects of background density on the Zöllner illusion. *Vision Research, 9*, 167–177.

Wallach, H. (1935). Über visuell wahrgenommene Bewegungsrichtung. *Psychologische Forschung, 20*, 325–380.

Weiss, Y., & Adelson, E. H. (1998). *Slow and smooth, a Bayesian theory for the combination of local motion signals in human vision*. AI Memo 1616, MIT.

Witkin, A. P. (1983). Scale-space filtering. In *Proceedings of the international joint conference on artificial intelligence* (pp. 1019–1022).

Wundt, W. (1898). Akademie der Sächsischen Wissenschaften Leipzig, Abhandlungen Die geometrisch-optischen Täuschungen. Abhandl. mathphys. der sachs. *Ges. Wiss., 24*, 53–178.

Yo, C., & Wilson, H. R. (1992). Moving 2D patterns capture the perceived direction of both lower and higher spatial frequencies. *Vision Research, 32*, 1263–1270.

Yuille, A., & Poggio, T. (1986). Scaling theorems for zero-crossings. *IEEE Transactions on Pattern Analysis and Machine Intelligence, 8*, 15–25.

Zeki, S. M. (1993). *A vision of the brain*. London: Blackwell.

Zöllner, F. (1860). Annalen der Physik und Chemie. Über eine neue Art von Pseudokopie und ihre Beziehungen zu den von Plateau and Oppel beschriebenen Bewegungsphänomenen. *Ann. Phys. Chem., 186*, 500–523.